

University of Uppsala, Angstrom laboratory
Faculty of Chemistry, Lägerhyddsvägen 1, 752 37
Department of Molecular Organic Chemistry, House 7



UPPSALA
UNIVERSITET

**Development of Multi-Linker Redox-Active MOFs for
study's on charge transport dynamics**

Roy B. Maas, 1095064

Organic Chemistry, Leiden University of Applied Sciences

Placement supervisor: Professor Sascha Ott
Daily supervisors: PhD students: Ashleigh Castner & Ben Johnson
Academic supervisor: Dr. Alphert Christina

June 17, 2019
From 1st of September till 30th June

Abstract

Om de potentie van katalysatoren ingebouwd in een redox actieve Metal–Organic framework (MOFs) volledig te benutten moet de charge transport / elektron hopping worden geoptimaliseerd. Voor het optimaal functioneren van een katalysator zal de drijfkracht achter het mechanisme van elektron hopping moeten worden onderzocht. Multi linker redox actieve MOFs werden gesynthetiseerd met een redox actieve (dcpOH–NDI) linker en een redox inactieve (dummy katalysator) dcpMe–BiPy. In deze thesis wordt elektron hopping als een functie van verschillende ratio's multi linker MOFs onderzocht. De afhankelijkheid van charge transport op de hoeveelheid redox actieve linker aanwezig in de MOF kan worden berekend in een electron diffusie coëfficiënt door middel van chronocoulometry en de Cottrel–vergelijking. De linkers werden gesynthetiseerd via

een condensatie reactie voor dcpOH–NDI en een Suzuki coupling voor de dcpMe–BiPy. Een kristallijne stof met ingegroeide kristallen, iconisch voor de UiO/PIZOF bevestigd met Röntgen diffractie en rasterelektronenscopie, werd verkregen uit een multi linker MOF synthese met 20% BiPy tot NDI ratio. 16% van de BiPy werd teruggevonden in het raamwerk met behulp van NMR. De thin film MOFs waren gesynthetiseerd voor electrochemische analyse in linker ratio's van 20, 50 en 80% dcpMe–BiPy waarvan, 23, 65 en 54% werd teruggevonden met NMR. Naast de afwijkende ratio's vormden de MOF films geen uniforme laag over het daarvoor bedoelde substraat, daarbij was de kristalliniteit laag bepaald röntgen diffractometrie (XRD). Uit rasterelektronenmicroscopie (SEM) bleek dat de topografie van de 20% BiPy ook sterk afwijkt van de 100% NDI thin film. De diffusie coëfficiënt(en) werden bepaald. Uit een tussen stap in de berekening bleek dat er meer NDI moleculen actief waren in de 65% NDI film dan in de 100% NDI thin film. Daarnaast vormden de coëfficiënten geen trend passend bij één van de mogelijke theorieën. De films waren ongeschikt om met elkaar te vergelijken. De factoren die waarschijnlijk een grote invloed hadden in de synthese zijn de concentratie van het reactie mengsel en de oplosbaarheid van de linkers. Dit werk brengt mogelijke obstakels beter inzicht en voegt toe aan de ontwikkeling voor multi linker MOFs.

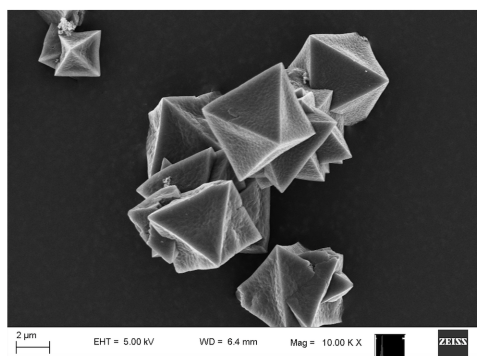


Figure 1: Foto van de MOF powder $Zr(dcpOH-NDI$ with 16% $dcpMe-BiPy$) met rasterelektronenscopie.

Table of content

List of Figures	v
List of Tables	1
1 Introduction	3
1.1 Redox active Metal Organic framework	3
1.1.1 Catalytic scaffold	3
1.1.2 Coordination polymer	4
1.1.3 Redox activity	5
1.1.4 Electron hopping	7
1.1.5 Form linker to MOF	8
1.1.6 Characterisation methods	10
2 Results and Discussion	15
2.1 Synthesis and Characterisation	15
2.1.1 Linkers	15
2.1.2 MOF Powders	16
2.1.3 SEM characterisation	19
2.1.4 Percolation threshold	20
3 Conclusion	23
4 Experimental section	25
4.1 Materials and Synthesis	25
4.1.1 Materials	25
4.1.2 Synthesis	25
4.1.3 Methodes and Procedures	27
5 Acknowledgements	29
Bibliography	31
6 Appendices	35
6.1 Appendix 1	35
6.2 Appendix 2	36
6.3 Appendix 3	37
6.4 Appendix 4	38
6.5 Appendix 5	39

6.6 Appendix 6 40

List of Figures

1	Foto van de MOF powder Zr(dcphOH–NDI with 16% dcphMe–BiPY) met rasterelektro-nenscopie.	i
1.1	Secondary building unit (SBU) of UiO–66 based on Zirconium, with carboxylate group bound to the cluster and chemical formula of the metal oxide cluster[1]	4
1.2	Electron transfer in homo–and heterogeneous medium driven by the energy difference between cobaltocene and an electrode that function here as electron donor made by El-grishi et al.(2017)	5
1.3	Unit cell of Zr(dcphOH-NDI) zirconium organic framework with the local charge carrier,NDI (naphtelene diimide) core highlighted in blue made by Johnson et al. (2018)	6
1.4	The redox active moiety, NDI undergoing a double reversable one electron reduction shown to delocalize the charge over its pi system.	7
1.5	An simplified view on electron hopping throughout the PIZOF reported by Johnson et al. (2018) where electron flow from the electrode on the left via the red linkers to the right to the blue linkers. Design by Johnson et al (2018)	8
1.6	Linkers used in the MOF synthesis, (A) OH–Phe, (B) OH–NDI and (C) Me–BiPy	8
1.7	A modeled formation of UiO–66 starting with the formation of the metal oxide clusters followed by the reaction with the linker (terephthalic acid) controlled by the equilibrium of association/dissociation between the modulator (acetic acid) and the linker with the metal clusters.[2]	9
1.8	A self assembled mono layer on a substrate resembling the FTO glass and the symmet-rical linkers binding to the substrate with carboxylate groups and presenting nucleation sides with the R–groups made by Vladsinger (2007)	9
1.9	XRD Patterns of Crystalline and amorphous materials[3]	11
1.10	CV form Ben A. Johnson et al (2018) of a two electron reversible reduction wave with $J / \text{mA cm}^{-2}$ current on the y–axis and potential in Volt on the X–axis referenced to ferrocenium / ferrocene standard.	12
1.11	Charge (Q/Coulomb) and current (i/Ampere) as a function of time over the potential steps of 0,6 v for 30 s, 1,08 v for 60 s and 0,6 v for 60 s again.	13
2.1	NMR of dcphOH–NDI	15
2.2	NMR of dcphMe–BiPy	16
2.3	Xrd results of the bulk MOF and of the thin film powders with the PIZOF reported by Johnson et al. and the simulated UiO–69 for comparison	17
2.4	NMR data from the digested bulk MOF modulated by acetic acid(upper spectrum Signal A= 25.23, B= 6.00) referenced to DMSO.	18

2.5	Thin films A(54% NDI),B(80% NDI),C(65% NDI),D(23% NDI) and the 100% NDI as a standard	19
2.6	Top view images made with SEM of film B and the 100% NDI film[4]	19
2.7	SEM image of the bulk powder sample showing a the interpenetrated octahedral reported by Johnson et al.	20
2.8	Charge (in coulomb) over time (s) plot of thin film C with trendline over the linear portion	20
2.9	Charge in coulomb over $t^{1/2}$ (s) of the 100% NDI film	21
2.10	The diffusion coefficient D_e in $\text{cm}^2 \text{s}^{-1}$ as a function of the concentration NDI in mol/cm^3 of the films	22
4.1	A schematic presentation of a one compartment three electrode setup.[5]	28
6.1	Formal electron diffusion (D_{app}) as a function of surface coverage of a redox active monolayer on conductive films (a)(TiO_2 , (c) Al_2O_3 in $\mu\text{mol}/\text{m}^2$ following a potential step from 0,2 to 1,0 v. The red arrow points a the onset of electron transfer.	35
6.2	NMR of the ester protected dcpHMe–BiPy	36
6.3	NMR of digested MOF powders resulting form the mixed thin film synthesis	38
6.4	SEM images of the crossection of the thin films B, C, D	39
6.5	Coulometry data of film B, C D, and the 100% film	40

List of Tables

2.1	Results of digestion ratio, SEM imaging and electrochemistry to calculate the formal electron diffusion D_e	21
4.1	List of the chemicals	25
4.2	summary of the Mixed linker MOF solutions of 80, 50 and 20% for thin film synthesis .	27

List of abbreviations and technical terms

MOF = Metal Organic Framework

PIZOF = Porous interpenetrated Zirconium organic framework

UiO-series = MOFs of a particular morphology first reported in the University of Oslo

Electron relay = A stable path way made of charge carriers which allow electrons to diffuse freely in between

TOF = turn over frequency, the rate at which a catalyst performs a catalytic cycle

SBU = secondary building unit, MOFs, consists of 2 primary building units, linkers and metal(oxide)clusters. The metal(oxide)clusters are the secondary building unit

Redox active = characteristic of a material or molecule to under go reduction and/or oxidation within a certain energy window (potential window)*

Redox inactive = characteristic of a material or molecule to be resistant to reduction and oxidation within a certain energy window.*

Percolation theory = theory that describes electron transfer behavior between charge carriers as being distance dependent

Localized charge carrier = a moiety that is fixed in space which is able to accept charges

Sacrificial electron donor = molecules that undergoes a non reversible oxidation reducing or donating its electrons in the process.

Fotosensitizer = Molecule that absorbs light produces high energetic electrons

TON = turn over number, the amount of catalytic cycles a catalyst performs on average before it deactivates

Reduction standard potential= energy at which a molecule accepts or donates an electron

FTO = Transparent conductive layer of fluor-doped tin oxide

SAM = self assembled monolayer

DMF = N,N-dimethylformamide

DME = 1,2-dimethoxyethane

MeOH = methanol

THF = tetrahydrofuran

* 'reduction and Oxidation' is used to refer to electron transfer to and from molecules, not a chemical process.

1. *Introduction*

1.1 **Redox active Metal Organic framework**

1.1.1 **Catalytic scaffold**

Artificial photosynthesis is a research field where the goal is to drive chemical processes using light, reducing the use of fossil fuels for energy for example. In nature the role of the light is to supply energy to electrons upon which they can be transported via charge carriers designated as an electron relay. Via iron–sulphur clusters the electrons are shuttled to be used in catalytic processes.[6][7] Using this phenomenon as inspiration a redox active metal organic framework was reported by Ben Johnson et al. (2018) which uses synthetic charge carriers that mimic the iron–sulphur clusters and facilitate this electron transport.[4] Redox activity is understood in electrochemistry as molecules that are able to undergo reduction and or oxidation. Metal organic frameworks, MOFs in short are crystal structures made from organic molecules and metal ions. These molecules coordinate like bidentate ligands to the metal centers linking them to each other. The electron transport, like in nature, has the potential to drive electrocatalyses because the electrons could activate the catalyst incorporated in the MOF. Electrocatalyses is a catalytic reaction where electrons are consumed or released during the process of forming oxygen and hydrogen for example from the splitting of water. For electrocatalysts to work optimally, assuming the substrate is present in abundance, the electron transport needs to meet or exceed the speed at which the catalyst turns over. This turn over frequency (TOF) is the speed at which a catalyst catalyses a reaction cycle and thus determines the amount of electrons it needs to accept or donate (depending on the catalyst) per second to function to its maximum capacity. In this MOF there is by design a fixed amount of space for both the charge carrier and dummy catalyst available. A dummy–catalyst is a molecule that is similar in characteristics to a catalyst but does not display any catalytic activity used to study electron transfer in isolation. Both the dummy–catalyst and charge carrier compete for a spot in the framework. In optimal conditions more catalyst will yield more product. But the electron transport which enables the catalyst can only occur if the charge carriers form a network to shuttle electrons through the framework. The formation of a network is proposed to be dependent on the distance between the charge carriers.[8][9] Dummy–catalyst incorporation effects the average distance between charge carriers assuming a homogeneous distribution by taking up space. To determine the minimal average distance required for electrons to move readily between charge carriers and thus the upper limit of catalyst incorporation, MOFs will be produced with varying charge carrier concentration and studied for their hopping capabilities using electrochemical analyzes. The formal electron diffusion obtained from the analyses will be reported as a function of the relative concentration of charge carriers in the MOF.

1.1.2 Coordination polymer

Metal-organic frameworks (MOFs) also known as coordination polymers is a result of Reticular Chemistry. This fast growing field, triggered in 1998 with the first reported porous MOF by Yaghi et al.[10], uses organic molecules that act as linkers and metal ions in clusters known as secondary building units (SBUs). Together they form structures that are upheld by coordination of the linkers to the metal ions. before this coordination, the metal ions react with residual water through a process not fully understood and form a metal oxide cluster see Figure 1.1. Because metaloxide cluster formation precedes the linker association during synthesis the orbitals of the metals are already partially filled up by oxygen oxo-bridges which hold the cluster of metalions together. The coordination of both the oxygen originating from the residual water and the linkers is based on metal-organic chemistry meaning that the metal in most cases needs to satisfy the 18-electron rule. The structure of the nodes templates how and how many linkers can associate. Near complete coordination of the linkers is vital for the crystallinity and thus the stability. Linkers are generally double or multi dentate organic ligands containing heteroatoms like oxygen or nitrogen on either end of the molecule. The lone pairs of these atoms can fill the the vacant sites of metal, coordinating into the empty orbitals. Just like Organometallic complexes have a particular three dimensional structure MOFs obtain their crystal structure as a result of crystal field theory.

Stability. Loss of coordinating ligand/linkers causes structural destabilisation in complexes and MOFs alike. Missing linkers or long extended linkers create bigger pore sizes.[11] Bigger pore sizes yield larges open cavities leaving the crystal prone to collapse upon removal of guest molecules like solvent residing in the pores.[11] Another phenomenon as a result of larger pore sizes is interpenetrated crystal growth. This has been observed by Johnson et al. (2018) in a UiO-based (University of Oslo) MOF using zirconium, designated as porous interpenetrated zirconium organic framework (PIZOF). The UiO-series is a class of MOF with a stoichiometry of one to one linker : zirconium forming a unit cell that consists of 1 octahedral flanked by eight tetrahedrals. By filling up the larger pores interpenetration stabilizes the PIZOF. In Figure 1.1 the SBU of UiO series is shown with 12 carboxylates anions in black and red coordinated to 6 zirconium ions in green held together by bridging Oxygens in magenta and lilac. Every carboxylate group binds to two different zirconium ions within the same metaloxide cluster. This greatly enhances the stability of the framework since complete linker dissociates depends on four metal-oxygen bonds.

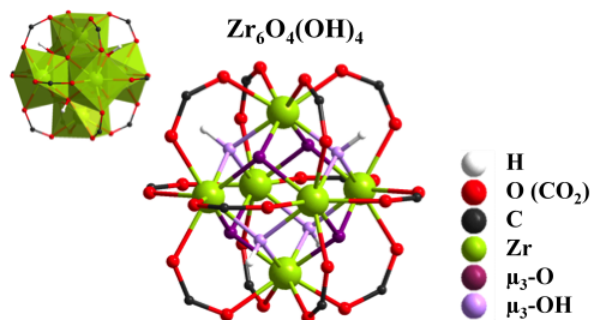


Figure 1.1: Secondary building unit (SBU) of UiO-66 based on Zirconium, with carboxylate group bound to the cluster and chemical formula of the metal oxide cluster[1]

Adaptable. The structural stability of most MOFs allows for the possibility to undergo post synthetic exchange (PSE) making them very versatile even after synthesis, resulting in a great amount of applications.[12] PSE is a method employed to introduce new linkers of the same length into the framework.[13] Often these newly introduced linker contain some extra functionality that the parent

MOF doesn't have of its own. for example, a catalyst functionalized linker that isn't stable towards higher temperatures couldn't be incorporated during the MOF synthesis but could with PSE. The exchange of the linkers is controlled by an equilibrium between association and dissociation of both the replaced and replacing linker. PSE and the many different metals and linkers available lead to a large array of different MOFs over the years with unique properties.[12] A feature that most of them share is a high surface area. The porous crystal structure expose the linkers and nodes buried deep in the crystal to a confined but open space. Diffusion allows for guest molecules like gasses or solvents to move in and out and interact through physisorption and chemisorption with the linkers or metaloxide nodes. Interaction through polarity, ionisation or through bond formation via a chemical reaction packs guest the molecules together. This application attracts lots of research because storage for gasses like hydrogen could help meet the demand for alternative energy sources for transportation instead of fossil fuels.[14]

1.1.3 Redox activity

A more recent field that attracts attention in MOF development is creating a redox active frameworks. Redox activity is understood in electrochemistry as molecules that are able to undergo reduction and or oxidation.

Electrochemistry. Redox processes entale an electron transfer from the reductor to the oxidant and visa versa. In Figure 1.2 an electron transfer of ferrocenium (Fc^+) and cobaltocene ($\text{Co}(\text{Cp}^*)_2$) and ferrocenium (Fc^+) to an electrode are shown. In both cases ferrocenium (Fc^+) is reduced by either cobaltocene or the electrode to ferrocene (Fc). The negative charge induced by the electron is stabilised by either counterions or an counterelectrode leaving the overall charge neutral. Both these reductions are driven by the tendency of nature to organize itself in the lowest amount of energy. On contact of (Fc^+) with ($\text{Co}(\text{Cp}^*)_2$) or the electrode an electron transfers to reside in the lowest possible energy state. In a solution of the redox couple ($\text{Fc}(\text{Fc}^+)$) electron transfer goes on continuously via a self exchange rate. This process is like a continuous equilibrium and can take place because the energy of the electron does

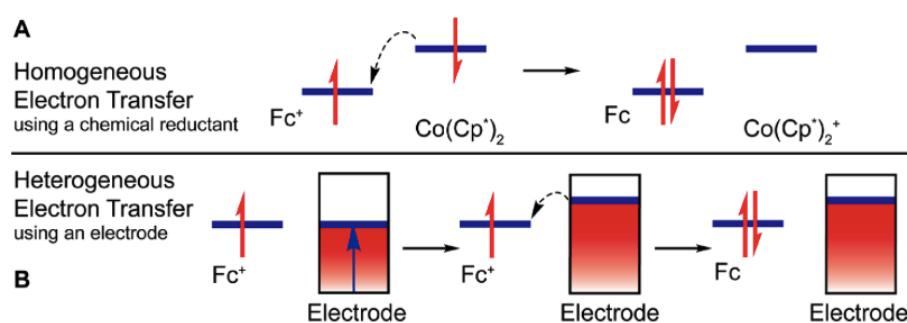


Figure 1.2: Electron transfer in homo–and heterogeneous medium driven by the energy difference between cobaltocene and an electrode that function here as electron donor made by Elgrishi et al.(2017)

not change at each transfer.

Redox active MOFs. By design MOFs are originally regarded as insulators. The linkers do not form conjugated π -systems, do not form channels through π -stacking and the metal ions can not undergo reduction or oxidation without the risk of losing stability due to linker dissociation. But electron transfer can occur upon introduction of metals like iron or cobalt into MOFs that accept and donate electrons like a ferrocenium/ferrocene couple.[?]][15] To ensure conductivity and the possibility to measure the redox activity of a MOF, MOFs are adhered to electrodes. Johnson et al. achieved this by growing the

MOF directly on a conductive support/substrate. It must be specified that these reduction/oxidation do not entail chemical reactions, only electron transfer seen between iron (III)/ iron (II) for example.

Electrocatalyses. Redox active MOFs open the doors for more efficient electrocatalyses like the reduction of protons to hydrogen in MOFs. Electrocatalyses in MOFs already attracted some attention because catalysts were shown to be stabilized upon immobilization into the framework impeding the degradation processes, extending its lifetime and thus its turn over number (TON).[13] but, catalysts like iron-ironhydrogenase used to be activated using molecules like sacrificial electron donors that donate an electron undergoing an irreversible oxidation itself.[13]

Delivering electrons. These electrons were supplied with energy via strong reductants or photosensitizer. Like nature's creation, chlorophyll, photosensitizers use light to create and deliver an energetic electron to the catalyst. The drawback of this method for driving electrocatalyses in MOFs is that the reductants need to diffuse into the MOF through the channels to reach the catalyst buried within the crystal. Depending on the size of the reductant and the pores of the MOF activation could be limited to only the catalyst close to the surface of the electrolyte due to steric hindrance upon diffusing into the framework.[16] With electrons able to move through the framework via the charge carriers that pass on electrons via a consecutive reduction and oxidation to "power" all catalysts, higher numbers of active catalyst are expected in comparison with the homogeneous analogue of the catalyst.

NDI. The NDI moiety able to mimic the iron-sulphur cluster used by Johnson et al., displayed in Figure 1.3, is a common organic electron acceptor[17].

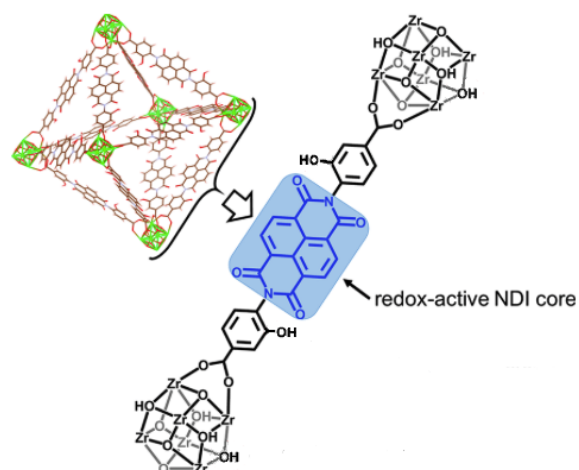


Figure 1.3: Unit cell of Zr(dcpHOH-NDI) zirconium organic framework with the local charge carrier, NDI (naphthalene diimide) core highlighted in blue made by Johnson et al. (2018)

The unique functional group, the imide consists of a five atom system where two carbonyls are joined together by nitrogen. In NDI, naphthalene diimide, two of these groups are joined together by naphthalene, a bicyclic aromatic compound forming a large π -system that is electron poor due to the higher electron negativity of the oxygen and the nitrogen on either side. These two properties allow for the delocalization of up to two electrons accepted in the LUMO displayed in Figure 1.4 below and is the reason that NDI is able to accept electrons. Just in the same way the redox couple (Fc)(Fc⁺) undergoes a self exchange process NDI does this to and is responsible for the electrontransfer in the PIZOF reported by Johnson et al.

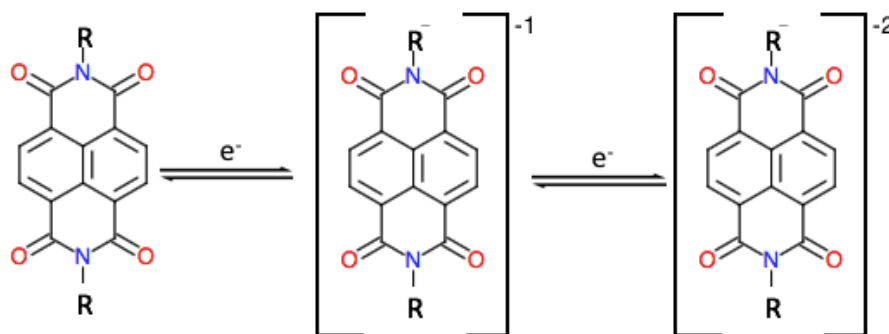


Figure 1.4: The redox active moiety, NDI undergoing a double reversible one electron reduction shown to delocalize the charge over its pi system.

1.1.4 Electron hopping

When charge carriers like NDI are build into a MOF there is a important difference with redox activity in solution, that changes the mechanism of electron transfer. The structure is rigid and the molecules are separated throughout the framework "stuck" in the crystal lattice. For electrons to "hop" to the now *localized* charge carrier within the MOF via self exchange the destination must be charge-balanced by counterions. Trough electron tunneling or cation coupled electron transfer, the electron need to overcome the energy barrier and arrives at the (next) carrier. Cations stabilize the negative charge like sodium ions stabilize chlorine ions. The electron hopping phenomenon is only observed within the presence of electrolyte where cations stabilize the reduced localized charge carriers.

Mechanism. The electron hopping process observed in charge carriers immobilized on polymers was described with LAS equation 1.1[18] in 1980.

$$D_{app} = k_{ex} \delta^2 C / 6 \quad (1.1)$$

Where the formal electron diffusion (D_{app}) through the polymer is a function of the distance (δ^2) times the concentration (C) of the charge carrier. This equation shows a linear dependence of formal electron diffusion over the charge carriers on the distance between the charge carriers.[19] The flexibility of polymers is believed to have a large influence on the electron hopping process because in more rigid systems, like monolayers of redox active molecules on metal oxide films, the relation between the formal electron diffusion is not linear but displays an abrupt onset as a function of the density of the charge carriers.[20] This onset was designated as the percolation threshold of which the data is presented in Appendix 1.[20] Percolation theory shows an distance dependent self exchange rate which, postulated by N. Blauch (1993) is due to the characteristics of electron tunneling as a potentially important electron transfer pathway.[21] The dual nature of electrons allow them to over come energy barriers. The probability of penetration of the energy barrier, in this case, the distance between the charge carriers decreases exponentially with the width of the gap. Percolation theory factors this distance dependent probability in to the self exchange rate and the threshold is where the distance is to large and the current drops to zero. Since the discovery of electroactive MOFs and of electron hopping, there is still little know about the mechanism operating. In 2017, Morris et al. made thin films of UiO-67 with redox active ruthenium complex. The formal electron diffusion coefficient found was the same for all the samples although they varied in charge carrier loading's. To explain this Morris et al. opted that the range of charge carrier loading studied, was below the percolation threshold.

Percolation. For electron hopping to occur in a MOF the distance between localized charge carriers (d) inserted as a black double arrow in Figure 1.5 can not exceed the distance for ion coupled electron transfer (d_i) to occur. This distance (d_i) is dependent on the probability of electron tunneling but unknown and arbitrary since it depends the medium the electron needs to traverse to arrive at the next charge carrier. With 97% of the redox active linkers active in the UiO/PIZOF reported by Johnson et al (2018) this requirement is met, displayed in an simplified framework where the Red linkers are transferring electrons to the blue linkers in Figure 1.5. Since NDI, the localized charge carrier, is built into the linker itself which are bound in the crystal structure the average distance between them can only be changed by replacing said linkers with redox neutral linkers which are not able to facilitate electron hopping. This means "diluting" the concentration of the redox active/charge carrying linkers with redox inactive linkers within the framework. If the distance between redox active charge carriers does exceed distance (d_i), the framework is rendered redox inactive. [8][9] At some point in the separating the charge carriers the electron hopping process is impeded.

The percolation threshold is important for future electrocatalytic functionalization of the PIZOF. Incorporation of catalyst functionalized linkers replace the charge carrying linkers "diluting" and increasing the average distance of the localized charge carrier. At some point the incorporation of catalyst exceeds the percolation threshold rendering the framework redox inactive defeating the purpose of incorporating catalysts since electrocatalyst like Fe-Fe hydrogenase demand a supply of electrons to reduce protons to hydrogen.[13]

1.1.5 Form linker to MOF

Linkers. To simulate this catalyst incorporation into the UiO/PIZOF the linkers in Figure 1.6 will be synthesized first. Linkers (A)(C), shown in Figure 1.6 are chosen since they are of similar length to dphOH-NDI (B), the Linker used by Johnson et al (2018), and do not introduce additional electronic effects like catalysts would. Aside from that dphMe-BiPy (C), the dummy-catalyst, does enable future electrocatalyst functionalization with cobalt through its lone pairs on the nitrogen atoms in the bipyridine moiety.[22][23] A major factor tying into why linker A and C were chosen is that they are redox inactive and do not undergo reduction in the same energy window as NDI does. Molecular orbital-theory explains this through the energy level of the lUMO of NDI which is lower in energy than those of ME-BiPy and OH-Phe. These linkers will be synthesized under argon atmosphere since their starting materials are oxygen or water sensitive via a Suzuki coupling for linker A and C and a condensation reaction for dphOH-NDI.

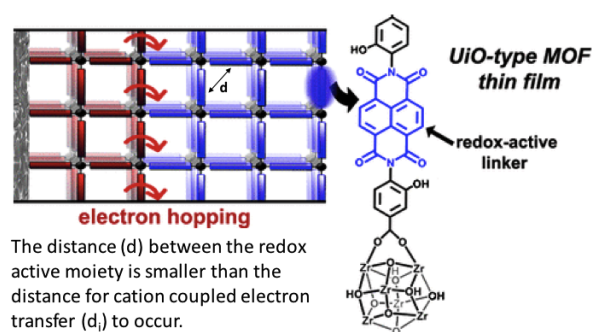


Figure 1.5: An simplified view on electron hopping throughout the PIZOF reported by Johnson et al. (2018) where electron flow from the electrode on the left via the red linkers to the right to the blue linkers. Design by Johnson et al (2018)

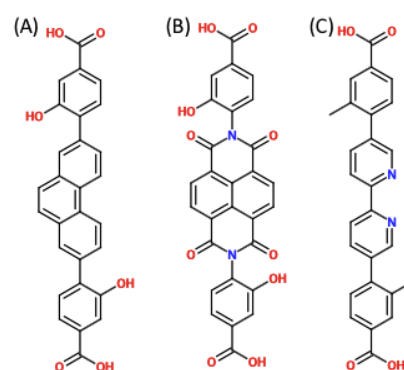


Figure 1.6: Linkers used in the MOF synthesis, (A) OH-Phe, (B) OH-NDI and (C) Me-BiPy

MOF. Secondly, the MOFs will be synthesized using the linkers in ratio between 20 to 100% redox active linker. The synthesis will be an adapted hydrothermal synthesis reported by Johnson et al. (2018) used for the PIZOF using acetic acid to regulate the reaction. Acetic acid plays the role of modulator during the synthesis. Most crystallization processes are a result of the solubility slowly decreasing giving molecules or ions time to precipitate in an orderly fashion. The UiO-MOF series along with many other MOFs are formed under high solvothermal conditions that facilitates the binding energy for linker coordination to occur.[15][24][25][26] This means that at the moment of sufficient (thermal)energy linkers start to coordinate randomly. The modulator comes in to deter the rate of linker association giving time for the crystal to arrange itself. The process is guided by an equilibrium of association and dissociation of both the modulator and the linker see Figure 1.7 as example for unit cell formation of UiO-66 with terephthalic acid and acetic acid. The driving force of

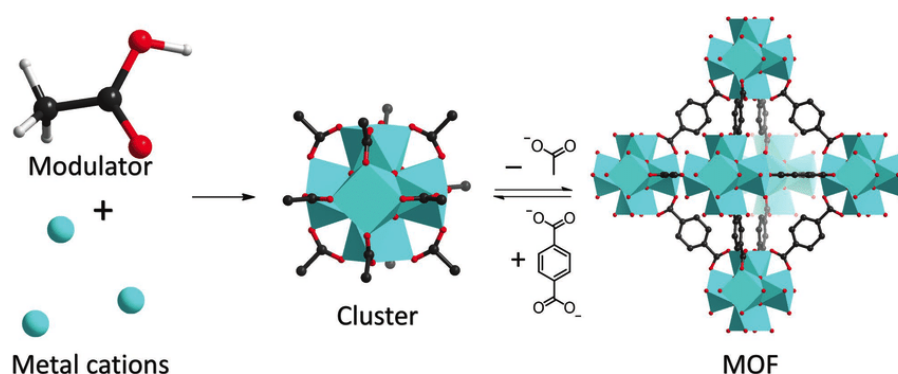


Figure 1.7: A modeled formation of UiO-66 starting with the formation of the metal oxide clusters followed by the reaction with the linker (terephthalic acid) controlled by the equilibrium of association/dissociation between the modulator (acetic acid) and the linker with the metal clusters.[2]

MOF formation is similar to most crystallization's using the tendency of matter to obtain the lowest energy state possible. At the same time, there is a constant competition between the modulator and the linker to associate to the metaloxide cluster. The size and the speed at which the crystal forms is greatly influenced by the concentration of the modulator. The more competition the slower the growth and so large crystals may be obtained.[27] Water, Brønsted acids and different modulator also influence the MOF formation opening a lot of optimization possibilities or variables during MOF synthesis.

Thin film. Lastly, the thin film mixed MOFs will be synthesized using a similar method as was used for the bulk MOF. Thin films are used for the electrochemical characterisation and zirconium frameworks have been shown to be stable.[4][28] To form crystals as a layer on top of a substrate known as a "support" in organic chemistry, a monolayer of the NDI linker is allowed to form on the fluor doped tin oxide layer of the glass slide. Formation of the monolayer grows by a self assembling process in solution also known as SAM (self assembling monolayer). In Figure 1.8 the substrate resembles FTO and both the head and the R-group carboxylates that bind to the surface

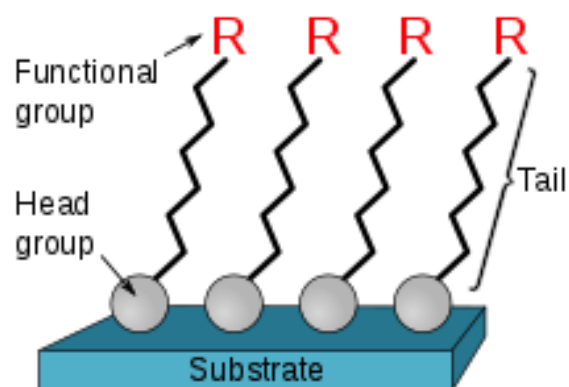


Figure 1.8: A self assembled mono layer on a substrate resembling the FTO glass and the symmetrical linkers binding to the substrate with carboxylate groups and presenting nucleation sides with the R-groups made by Vladsinger (2007)

with one end of the linker. These linkers act as anchor and nucleation side for crystals to grow on. Making use of a monolayer ensures better connectivity between the FTO and the MOF and so help prevent the MOF crystals from falling off the substrate. FTO is a transparent film that can conduct electrons and will be used as the electrode surface during electrochemical analyses. To study the percolation threshold of this UiO/PIZOF electrochemical analyses will be conducted on the thin film MOF grown on FTO.

This Thesis work is dedicated to establish an upper limit for future catalyst incorporation within the UiO/PIZOF reported by Johnson et al. by resolving the minimum concentration of redox active linkers relative to redox inactive linkers within that MOF required for percolation to occur.

1.1.6 Characterisation methods

The linkers will be characterized with Nuclear magnetic resonance (NMR) analyses. The characterisation of the MOFs will be done with Scanning electron microscopy (SEM), powder X-ray diffraction (PXRD) as well as NMR after digestion of the framework, meaning breaking the MOF down to the free linkers and SBU's. These techniques are mostly used as qualitative analyses except for NMR Measurements. After the digestion NMR analyses gives insight into the ratio of the incorporated linkers in the MOF. SEM and XRD data will be compared with well established MOFs.

X-ray diffraction

PXRD is a technique used for crystal structure analyses that provides information on the dimensions of the unitcell in periodically arranged crystals using X-rays. These X-rays are produced by a metal target like copper that is exposed to electrons generated by a heated filament. The generated electrons are focused with a voltage and are able to dislodge electrons from the inner shell of the metal. The atom reacts by filling up the empty orbital with an electron from the outer shell and in this process high energy photons are released which are monochromatized before they are directed at the sample. The monochromatic X-rays interact at certain angles that satisfy the Bragg's law (eq 1.2) with the crystal lattice and produce constructive interference characteristic for the particular lattice in question. The more regular the specific diffraction occurs the stronger the signal. The Bragg's law:

$$n\lambda = 2d \sin \theta \quad (1.2)$$

displays the relationship between the wave length (λ) to the interplanar distance (d) of the lattice and the angle of incident (θ). Data obtained from XRD analyses is visualized as diffraction intensity in counts per second as a function of 2θ . The name powder XRD is somewhat miss leading because non-powders will not yield constructive interference since there is no repetitive lattice for X-rays to interact with. Instead amorphous solids will display a broad scatter signal upon impingement by X-rays. A visual presentation is showed in Figure 1.9 where crystalline material is easily distinguished from amorphous material.

Scanning Electron Microscopy (SEM)

SEM is a technique used to take images of materials on micro and nanometer scale. This type of analysis gives information on surface topography. As the name implies, the techniques scans electrons that come

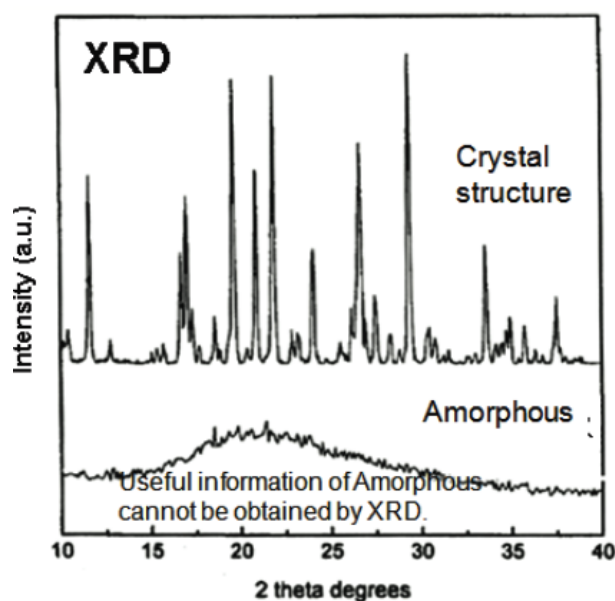


Figure 1.9: XRD Patterns of Crystalline and amorphous materials[3]

off the surface of the sample, collects them on a detector and translate it to an image. These electrons are agitated by the beam coming from the source for example a tungsten filament. The electrons from the beam impact the sample and interact with the atoms on the surface in three different ways. Two of these mechanisms force an electron out of the atom which is detected. Depending on the depth of impact in the atom this is paired with the emission of high energetic photons as a result of electrons filling up orbitals of lower energy levels. The other mechanism where the same electron emitted from the filament is detected is a result of interaction with the nuclei. All these processes occur more readily with heavier elements since their outer electrons are lower in energy and thus less strongly bound to the nucleus because the nuclei are more shielded because it is bigger and carries more positive charges. For this reason samples with higher content of lighter elements are sputter coated with heavier elements like palladium gold alloys. An obvious side effect of using an electron beam on samples is static charge accumulation that influences the measurement. To avoid this samples are mounted on or connected to a conductive surface like conductive carbon. The images can be used to compare the exterior of the films to that of the PIZOF.[4] Once concluded that the material is a MOF the redox activity and percolation theory can be tested. This will be done by subjecting the films to Electrochemical analyses by cyclic voltammetry.

Cyclic Voltammetry

Cyclic voltammetry (CV) is a technique used to trigger and study electrochemical reactions, including probing the reaction mechanisms and kinetics. The reduction of NDI in thin films is driven by and followed with cyclic voltaic measurements where the 'working' electrode the FTO substrate injects electrons in to the framework. This technique measures the current (electrons passing between the electrode and the sample) over the scan range of the electrochemical process called the potential window. When the potential matches or exceeds the energy level of the LUMO of the redox active species electrons will flow in to the sample. If it is lower than the now occupied orbital of the reduced species electrons will

flow out of the sample. Both directions of electron flow is measured as the current that passes through at the certain potential. The current passing through the analyte/species is compared with the current found in the reference(electrode) or Fc/Fc^+ couple depending on the setup. This is important for comparisons, because there are many variables like, concentration of electrolyte, solvent and temperature that effect the redox features of the analyte. by referencing the analyses to a standard the different runs of measurements can be quantitatively compared to each other. The potential at which the analyte is reduced and oxidized is the standard potential. This value is acquired during the measurement by heterogeneous electron transfer between the electrode and the in this case NDI.

NDI. When the potential reaches the energy threshold (standard potential) NDI accepts an electron in to its lumo. Because the MOF consists out of charge carriers the propagation of electrons starts and the current increases. When the reduced species saturates the space around the electrode and the thin film is reduced the current decreases. Upon the reversal of the potential the earlier reduced species will be oxidized and deprived of their electrons. This flux of electrons is again measured and assuming the reduced species did not react in anyway other then accepting an electron a reversible wave will be observed where all prior reduced NDI now is oxidized

In Figure 1.10 two sequential one electron process is measured of the double reduction of NDI, scanning from positive potentials to negative potentials and back. The two double waves result from the reduction wave with negative current going form right to left and the oxidation wave with positive current going form left to right. In both waves there are two signals/current amplifications visible which correspond to the sequential double reduction and oxidation of NDI radical and the dianion NDI. The reduction of NDI as mentioned before is made possible with the association of cations. In order to stabilize reduced NDI the ions need to make their way through the framework. Over many cycles the number of cations in the framework increases hence the number of Reduced NDI increases so does the measured current. Figure 1.10 displays a multiple cycle color coded scan of PIZOF–NDI thin film from purple with the lowest current to red with the highest current. When more cations are available higher current is observed.

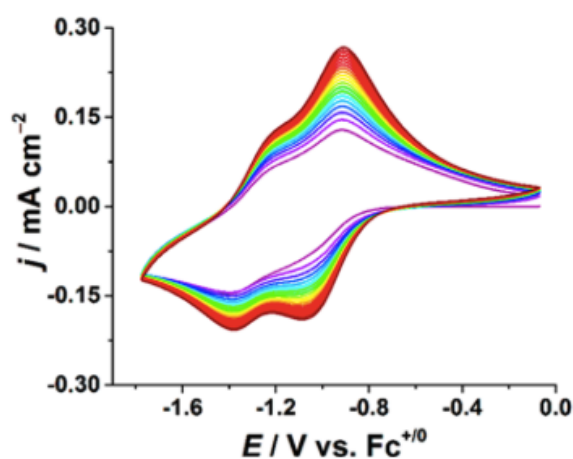


Figure 1.10: CV from Ben A. Johnson et al (2018) of a two electron reversible reduction wave with $J / \text{mA cm}^{-2}$ current on the y-axis and potential in Volt on the X-axis referenced to ferrocenium / ferrocene standard.

Chronocoulometry. To measure the formal electron diffusion the thin films have to be conditioned first using CV. During several cycles the framework is loaded with electrolyte to stabilize the charge carriers in the potential step analyses. In this analysis the potential is held constant for a set time periods. After conditioning the results of the step wise potential analyses can be used to calculate the formal electron diffusion using the Cottrell equation (eq. 1.3) as Morris et al. did.

$$i = \frac{FSC_{\text{NDI}}\sqrt{D_e}}{\sqrt{\pi t}} \quad (1.3)$$

Where (i) is the current at time (t), F is Faraday's constant, S is the surface area of the electrode C the concentration of the redox active species and D the formal diffusion. By measuring the first reduction changing the potential from 0.6 to 1.08 V and back monitoring the charge and current over time see Figure 1.11 the Cottrell equation could be solved for the formal electron diffusion (D_e). The concentration (C_{NDI}) can be calculated from the charge and the volume using SEM imaging to determine the film thickness. To obtain this data in Figure 1.11 the linkers have been synthesized.

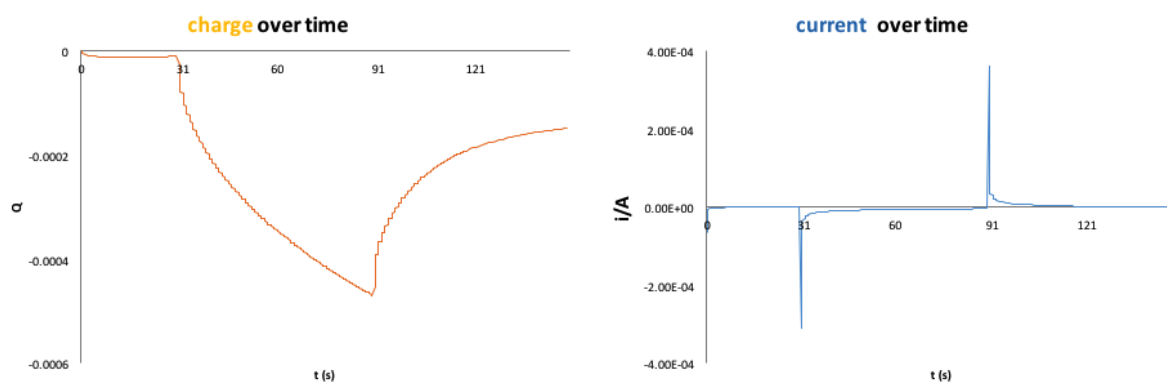


Figure 1.11: Charge (Q/Coulomb) and current (i/Ampere) as a function of time over the potential steps of 0,6 v for 30 s, 1,08 v for 60 s and 0,6 v for 60 s again.

2. Results and Discussion

2.1 Synthesis and Characterisation

2.1.1 Linkers

DcphOH–NDI. The carboxylic acid functionalized redox active linker dcphOH–NDI was synthesis via a double condensation of 1,4,5,8–naphthalenetetracarboxylic acid dianhydride with 4–amino–3–hydroxybenzoic acid in anhydrous DMF under argon. Earlier synthesis in older non–anhydrous DMF, single and double hydrated naphthalene 1,4,5,8–tetra carboxylic acid formed as a side product due to the hydration of the carboxylic acid anhydride by water present in the "wet" DMF. To circumvent this problem a Dean–stark reflux was initiated using toluene as solvent. However after 24 hours the starting materials were isolated most likely because of the poor solubility of the reagents in toluene. The final yield was 1.07 g, 66% and product was characterised with NMR see Figure 2.1. Note that protons of the carboxylic acid are not assigned in the NMR since they fall out of the ppm range displayed by the software.

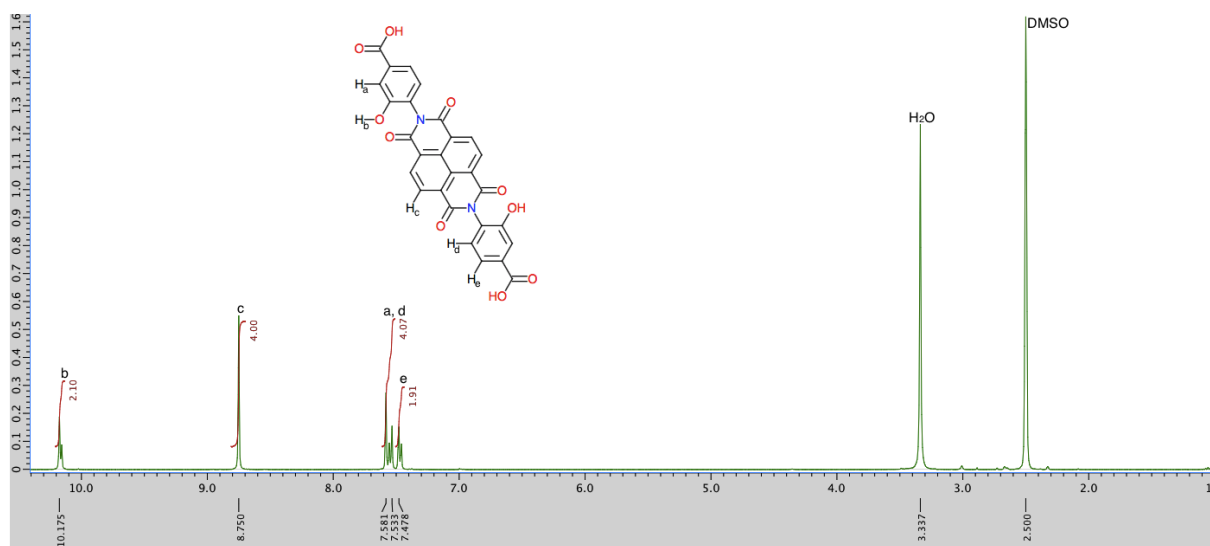


Figure 2.1: NMR of dcphOH–NDI

Redox inactive linker. Prior to the synthesis of dcphMe–BiPy a phenanthrene based linker (linker A in Figure 1.6 in the introduction) was chosen for redox inactive linker. This linker was initially chosen because of its presumed robustness towards redox chemistry and of its similar hydroxy group on the outer phenyl ring. Several attempts to synthesize this linker using a Suzuki coupling reaction in vain led to the decision to use dcphMe–BiPy which allows for catalyst incorporation via the bipyridine moiety. DcphMe–BiPy was synthesized using a microwave for 3 hours on 150° C via a Suzuki coupling reaction between 5,5'–dibromo–2,2'–bipyridine and 4–(methoxycarbonyl)–2–methylphenylboronic acid with

tetrakis(triphenylphosphine)Palladium in DME and water. Washing the gray product with cold water and extracting it by Soxhlet extraction with chloroform was followed by a saponification reaction with 6 M KOH solution to form the free acid linker. The final yield was 43,1 mg 14,8% and characterized with NMR see Figure 2.2. The final product show impurities around 1.5 and 3.4 ppm that are attributed to residual solvents and an "wet" bottle of DMSO-d₆. The NMR of the ester protected linker isolated from the Suzuki coupling is shown in Appendix 2. The reaction mechanisms of both products can be found in Appendix 3.

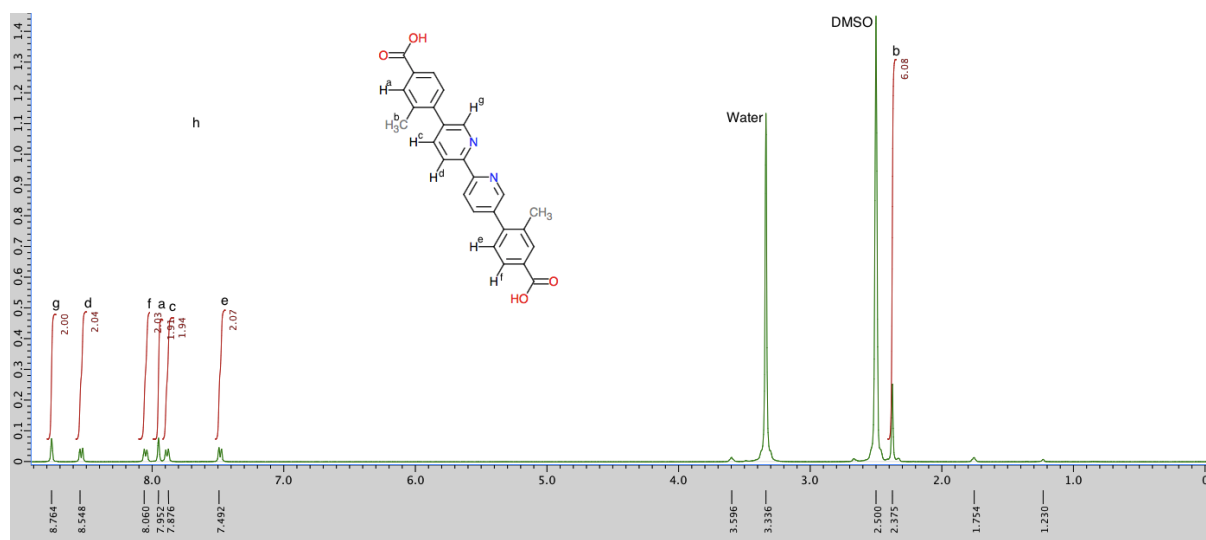


Figure 2.2: NMR of dphMe-BiPy

2.1.2 MOF Powders

powder-XRD characterisation. These linkers were used in a ratio 1:4 dphMe-BiPy : dphOH-NDI in a bulk MOF synthesis with ZrCl₄ and acetic acid as modulator. DphMe-BiPy did not readily dissolve and resulted in a turbid solution. The powder that formed was analysed with XRD (Figure 2.3). The spectra of the PIZOF reported by Johnson et al. and UiO-69 are included for comparison. In essence the PIZOF reported by Johnson et al. is based on UiO-69 but as stated before, the longer linkers result in larger cavities allowing interpenetrated crystal growth.[26] This interpenetration changes the diffraction angles giving rise to a different XRD pattern. The crystal structure of the bulk synthesis is expected to resemble the PIZOF because the reaction conditions are similar and the linkers are approximately the same length. The high intensities at the same diffraction angles of the Bulk powder suggests high crystallinity.

Thin film powders. The powder that formed in the B(80), C(50) and D(20% NDI) thin film synthesis was also subjected to XRD analyses. The data was added in Figure 2.3. The diffraction signals of the thin film powder samples are significantly different from the bulk MOF synthesized sample, the PIZOF and the UiO-69. The powder shows broad signals and high background which indicate that the powder has more amorphous characteristics than the PIZOF or the Bulk Powder do. Pore collapse could have occurred. main causes for this are: extraction of supporting guest molecules or formation of less crystalline material during the synthesis. Collapse due to guest molecule removal is not the case here as the MOF samples were not subjected to a vacuum to remove the solvent from the framework. The differences between the the reaction conditions of the thin film and the bulk MOF synthesis however could have been the cause for this lower crystallinity. The concentration of the linkers and zirconium

and the amount of modulator were different between both syntheses. The thin film and the powder is formed in 12,5 mM of zirconiumchloride in DMF with 30 equivalent of modulator. The bulk MOF with 16% BiPY was formed in 87,5 mM zirconiumchloride₄ and 45 equivalent of modulator. The linker ratio's of the bulk MOF and the thin film synthesis, A and B were the same.

Crystal formation factors. Lower amounts of modulator result in faster coordination. Low crystallinity could have been a result of improper control of the growth rate. On another note, a lack of interpenetration could also destabilize the framework. Turbid solutions and the low concentration can have affect on the frequency of interpenetration happening. With regulation of the crystal growth, the modulator can effect the size of the crystals but it can also increase linker defects within the unit cells.[29] fewer coordinating linkers lower the structural support of the framework and leaves it more prone to collapse.[2] The PIZOF reported by Johnson et al. with only dcpOH–NDI as linker was formed and stable using 30 equivalent of modulator.[4] The introduction the second linker with not exactly the same length (20,25 Å) as OH–NDI (20,63 Å) could put stress on the SBU's because of slight deviation in distance. These factors, less growth regulation from the modulator and the minor distance variation of the linkers and concentration combined might have rendered the MOF powder unstable if it could have formed at all. film A and B had similar molar ratio's of the two linkers as in the bulk powder which does show high crystallinity.

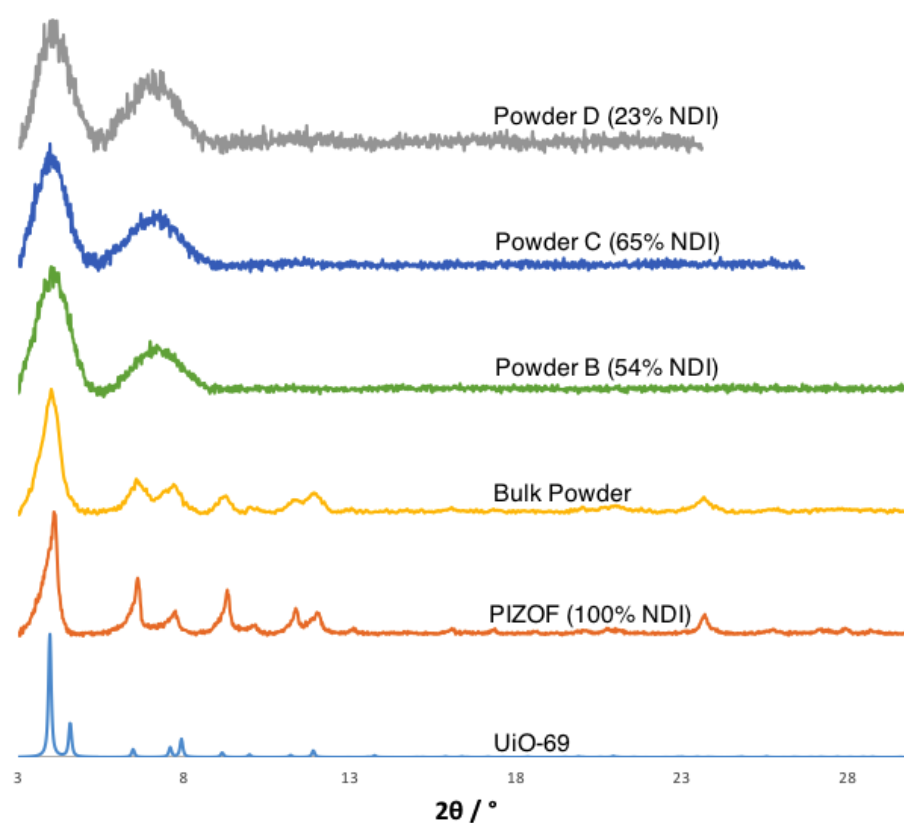


Figure 2.3: Xrd results of the bulk MOF and of the thin film powders with the PIZOF reported by Johnson et al. and the simulated UiO–69 for comparison

Linker incorporation. Linker incorporation calculation were done on the digested bulk MOF powder with hydrofluoric acid and NMR analyses. Approximately 16% of dcpMe–BiPy was incorporated in the sample of the bulk MOF synthesis. This ratio is derived from the integrals belonging to the two linkers. The signals chosen For dcpOH–NDI were the protons on the naphthalene core in the NDI

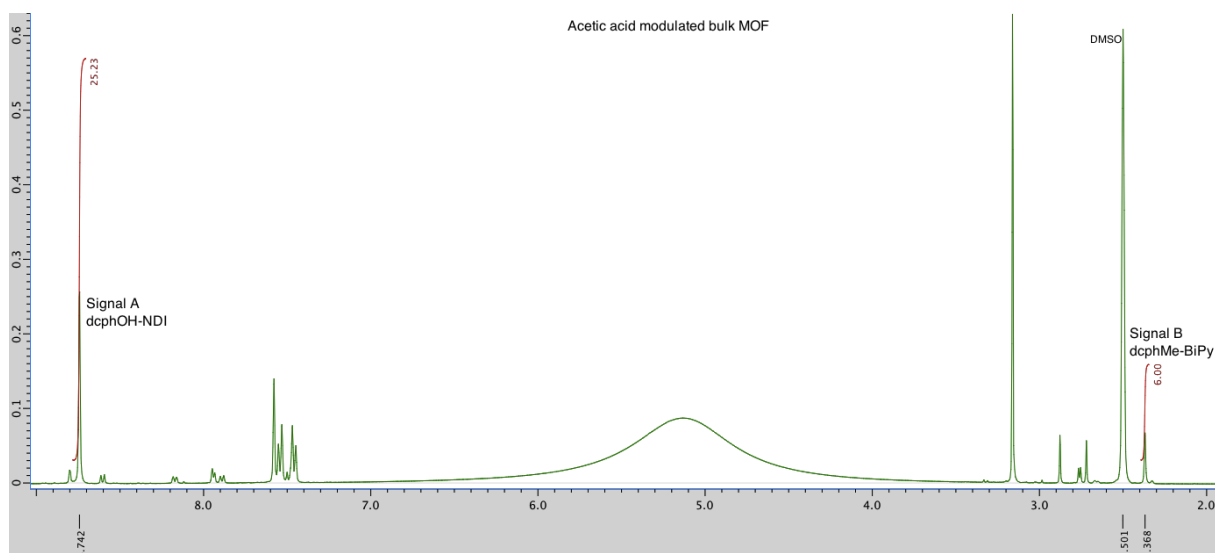


Figure 2.4: NMR data from the digested bulk MOF modulated by acetic acid(upper spectrum Signal A= 25.23, B= 6.00) referenced to DMSO.

moiety around 8.74 ppm and the Methyl group protons at 2.34 ppm on the benzoic acid moiety of the dcpMe–BiPy since they do not overlap, are easily identified and characteristic. First, the signals are normalized by dividing the integrals by their respective amount of protons equal to that in the free linker shown in equation 1 of the acetic acid modulated MOF. This yields a percentage of the linker present in the lowest concentration of the two within the PIZOF.

$$\frac{\text{integral}(6)}{\text{corresponding protons}(6)} = 1$$

$$\frac{\text{integral}(25.23)}{\text{corresponding protons}(4)} = 6.3075$$

$$\frac{1}{6.3075} \times 100 = 15.857\%$$

To determine the ratio of the less crystalline MOF powder samples from the Thin film synthesis the same procedure was applied. The incorporation of dcpOH–NDI was 54%, 65% and 23 for synthesis A, C and D with 80, 50 and 20% as expected by molar ratio respectively. The NMR of these digested samples can be found in Appendix 4. The ratio's found for the A and C are not in line with the expected value's. Although deriving the ratio from the NMR is a rough estimation, the difference of the ratio's is larger in film A and C than the expected errors of signal integration. Combined with the XRD results for the powders before digestion, the formation process of the materials did not treat both of these two linkers equally. which isn't unexpected because the difference in solubility. Since the MOF reaction mixtures were turbid, nucleation of the MOF most likely started with incorporation of dcpOH–NDI opposed to dcpMe–BiPy, because it was readily available due its higher solubility. Other factors effecting the incorporation ratio is a non–homogeneous distribution of the linkers as a result of again the difference in solubility of both linkers during synthesis. It is expected in most crystal formation processes that the material in question is fully dissolved. With the seemingly little differences in the synthesis conditions between the bulk and the thin film and the large difference in the thin film formation it is remarkable that the bulk synthesis yielded MOF crystals out of a turbid reaction mixture with 16% BiPY linker incorporated.

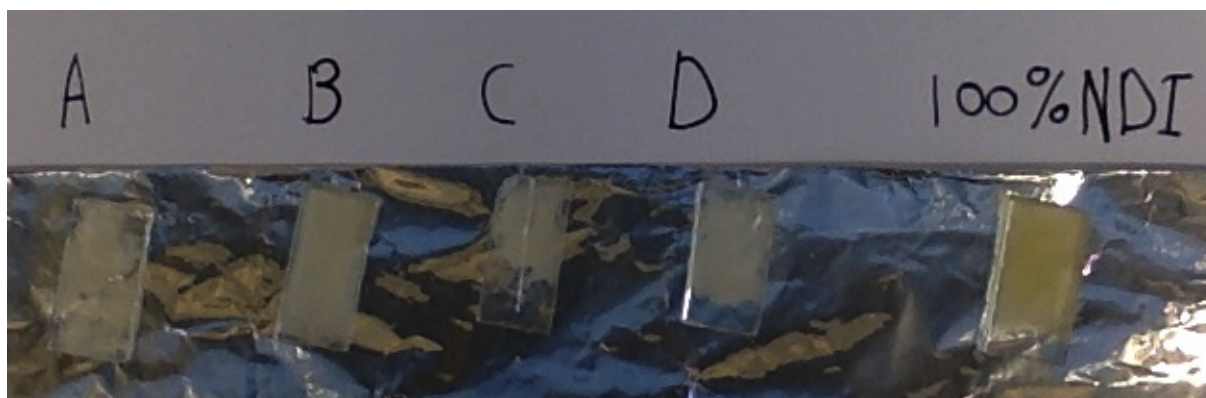


Figure 2.5: Thin films A(54% NDI),B("80"% NDI),C(65% NDI),D(23% NDI) and the 100% NDI as a standard

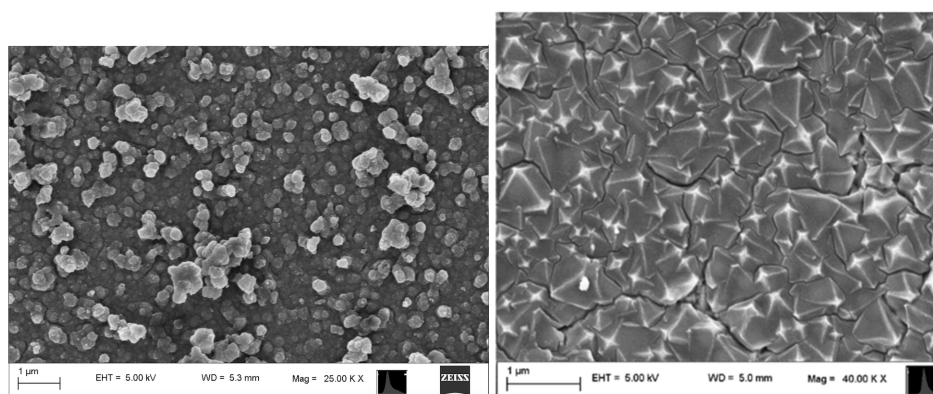


Figure 2.6: Top view images made with SEM of film B and the 100% NDI film[4]

2.1.3 SEM characterisation

Thin films. In total 5 different thin films were synthesized in two fold and characterized with SEM. As a control one of these was the reported 100% NDI thin film by Johnson. With the same procedure and total concentration as the 100% NDI PIZOF, thin films A/B, C and D were synthesized with dcpOH–NDI and dcpMe–BiPY in ratio's of (4:1) 80% NDI ,(1:1) 50% NDI and (1:4) 20% NDI respectively. The FTO glass slides used were stored in a non-ventilated area for 6 months before use. The films didn't form homogeneously over the FTO like the 100% NDI PIZOF does. See Figure 2.5 Films B, C, D and 100% were subjected to electrochemistry. As mentioned the reaction mixtures used to produce the films as well as the powder was turbid. The turbid solution prevents even nucleation over the films. Which makes a non homogeneous distribution of both linkers likely. Film A was synthesized again but this time with half of the concentration of linkers and zirconium yielding a clear reaction mixture and a homogeneously covered film (B). SEM imaging of film B compared to the 100% NDI showed that the film didn't adopt the topology of the of the 100% NDI however it seems to have formed a consistent irregular film see Figure 2.6. Although the topology does not resemble the UiO/PIZOF, the material might still be porous. But there is a clear distinction in morphology between the films which might influence the electrochemical analyses. The same goes for the cross section images were the thin films are very irregular see Appendix 5. The film thickness could vary with in a single film ranging form 5 to 1 μm (film D). An explanation for the non-homogeneous films might be either dust that accumulated and stuck to the FTO even after washing or the high concentration that yielded turbid reaction mixtures denying proper crystal formation. Lower concentrations like in film B didn't allow for regular crystals to grow,

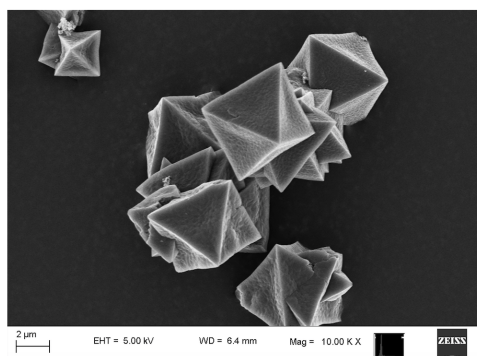


Figure 2.7: SEM image of the bulk powder sample showing a the interpenetrated octahedral reported by Johnson et al.

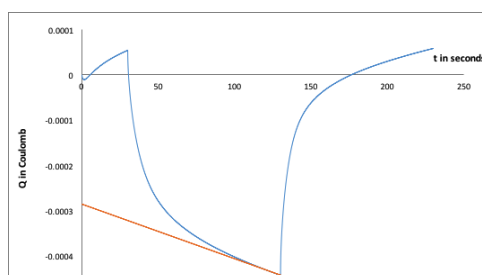


Figure 2.8: Charge (in coulomb) over time (s) plot of thin film C with trendline over the linear portion

in comparison with what has been seen in the bulk powder synthesis. This synthesis approach seems to be limited in the sense that larger amounts of dphMe–BiPY do not readily dissolve. This Likely resulted in a non homogeneous distribution and obstruction of nucleation and irregular film thicknesses. Nevertheless the film thickness was approximated with the software for percolation calculations. To form homogeneous films, turbid mixtures should be avoided since they produce inconsistent results. But the concentration needs to be high enough for crystals to fully form. The film thickness from the cross section images is determined from the SEM images in Appendix 5 as: film B = 0,00013, C = 0,00012 D = 0,00033 and 100% NDI = 0,0001 cm.[4]

Powders. The bulk powder of 16% BiPY linker formed in a turbid 85,5 mM solution, were thin films are made in 12,5 mM, did form crystals seen in Figure 2.7 confirming the results from the XRD analyzes.

2.1.4 Percolation threshold

The thin films 100%, B, C and D were subjected to a potential window from 0,0 to -1,08 v with respect to Ag/Ag(NO₃) reference electrode referenced to ferrocenium/ferrocene (Fc⁺⁰) couple about 0.06 v versus Ag/AgNO₃. First, the films were conditioned with cyclic voltammetry until the current didn't increase any longer with every subsequent scan because more NDI is able to be stabilized by the accumulating electrolyte in the MOF. After multiple cycles the films are subjected to a potential jumps to induce the first reduction of the NDI and the following oxidation. During these analyses the charge and the current are measured over time see Figure 1.11 in the introduction and Appendix 6.

With the charge and the current the Cottrel equation can be solved for the formal diffusion (D_e).

$$i = \frac{FSC_{\text{NDI}}\sqrt{D_e}}{\sqrt{\pi t}} \quad (2.1)$$

The total amount of charge that goes into the film is equal to the amount of mols NDI reduced. The

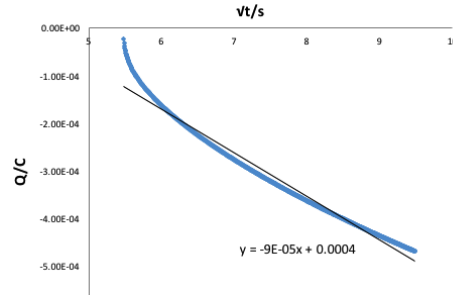


Figure 2.9: Charge in coulomb over $t^{1/2}$ (s) of the 100% NDI film

linear part of the charge time plot is a result of a phenomenon not relevant for the analyses but, of which the slope is used to calculate back to $t=0$. The total amount of charge is equal the charge at $t=0$ and the starting value right before the potential drop $t = 30$ second in the measurement. By dividing the total charge by Faraday's constant the mols of NDI that was redox active is obtained. Rewriting the Cottrell equation (eq 2.2) for charge (Q), the positive value of the slope of charge (Q) over $t^{1/2}$ in the reduction period between $t= 30$ to 130 seconds is equal to $\frac{2FSC_{\text{NDI}}\sqrt{D_e}}{\sqrt{\pi}}$.

$$Q = \frac{2FSC_{\text{NDI}}\sqrt{D_e}}{\sqrt{\pi}} \times \sqrt{t} \quad (2.2)$$

The concentration of NDI in the thin film is calculated by the division of the mols NDI on the surface area ($S \text{ cm}^2$) of the film times the average film thickness measured from the SEM imaging (Appendix 5).

with the slope, the concentration NDI and the film surface area the diffusion D_e can be calculated following equation 2.2 It is notable that the concentration of the NDI in film C(65%) measured with

Table 2.1: Results of digestion ratio, SEM imaging and electrochemistry to calculate the formal electron diffusion D_e

Thin film	B	C (65%)	D (23%)	100% NDI
Surface area (S in cm)	0,9	1,2	1	1
Film thickness (cm)	0,0001337	0,00012165	0,0003343	0,0001
OH-NDI (mol)	1,48E-9	3,51918E-9	2,9197E-9	1,66269E-9
Slope $Q/t^{1/2}$ plot	0,00005	0,00004	0,00003	0,00009
C NDI (mol/ml)	1,2307E-05	2,41073E-05	8,7196E-6	1,66269E-5
diffusion D_e (cm^2/s)	1,71914E-9	1,61294E-10	9,9863E-10	2,47183E-9

electrochemistry is higher than the number found for NDI in 100% PIZOF thin film. Since this analyses is quantitative for the total amount of charge that is injected into the framework. electrochemical analyses show there is more OH-NDI (in mols) present in the C (65% NDI) film than in the 100% NDI film. The NDI present in the films behaves very different depending on the presents of dcpHMe-BiPy and might not be directly comparable. The electron diffusion (D_e) is plotted against the concentration of NDI.

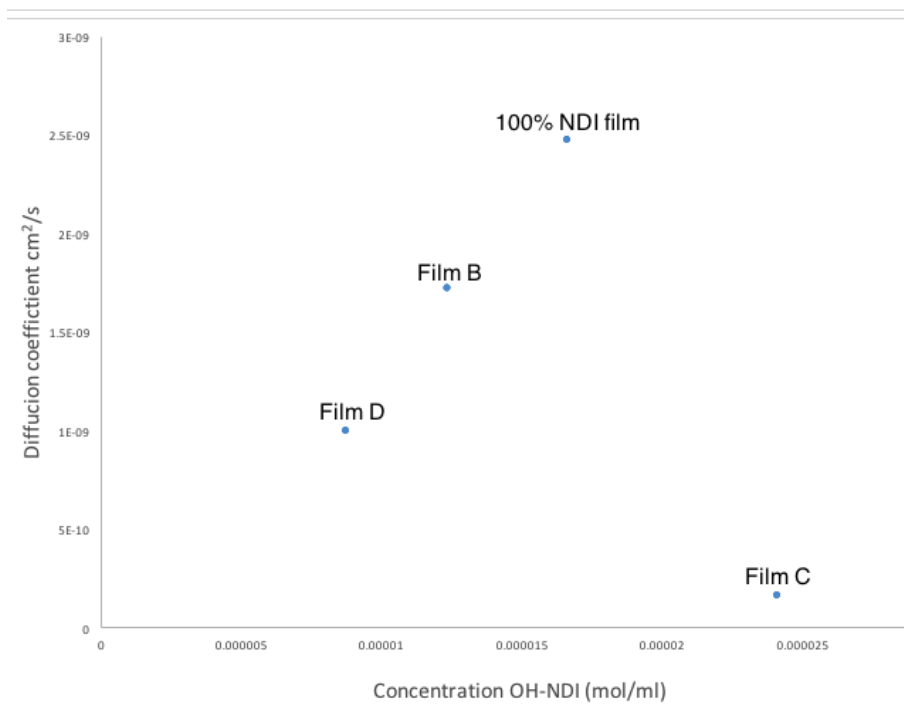


Figure 2.10: The diffusion coefficient D_e in $\text{cm}^2 \text{s}^{-1}$ as a function of the concentration NDI in mol/cm^3 of the films

The values found for the diffusion are in the same order of magnitude as reported by Jonson et al. But the diffusion coefficient (D_j) do to follow a trend with the concentration of redox active linker present which was determined as a parameter for the average distance between the charge carriers. It was expected according to percolation theory that the formal electron diffusion now the diffusion coefficient (D_j) would decrease dramatically with a lower concentrations. Neither is there an apparent linear relationship which is reported on polymer backbones. As shown by XRD and SEM analyzes the morphology changes upon incorporation of dcpHMe–BiPy in such a way that the amount of redox active linkers participating in the charge transport changes. Aside from that is the estimation of the film thickness from the cross-section with SEM unreliable. The film thickness has a large impact on the concentration of NDI in the film and thus on the electron diffusion. Since the film thickness varies a lot in the same film SEM, although accurate, does not give a good estimation of the total film coverage without randomized multiple samplings. Atomic force microscopy (AFM) or ellipsometry could be considered as alternatives for thickness analyzes. Both these techniques cover large areas resulting in more accurate thickness estimations.

3. *Conclusion*

The design of dual linker redox MOFs is an important step for applications in electrocatalyses. In this thesis redox active thin films based on the PIZOF reported by Johnson et al. have been made with a redox inactive linker that enable future catalyst functionalisation through the bipyridine moiety.[28]

Linkers. DcphOH–NDI was synthesized and obtained in decent yield and high purity. DcphMe–BiPy was synthesized in very low yield. In future a new synthetic path way may be constructed using Dichloro-Bis (aminophosphine) Palladium Complexes for it was reported to be a highly active Suzuki coupling catalyst .[30]

Powder. The linkers used in the bulk MOF synthesis in a molar ratio of 4:1 dcphOH–NDI: dcphMe–BiPy resulted in a 16% incorporation of BiPy linker in a PIZOF framework confirmed by XRD and SEM imaging.

Thin film. With the promising results of the bulk synthesis, thin films were made. The MOF films did not form homogeneously over the substrate. The SEM imaging showed a morphology of film B that differed from that of the 100% NDI reported by Johnson et al. and the low crystallinity of the corresponding powders points out there are many differences with the PIZOF of 100% NDI. The formal electron diffusion as a function of the concentration of NDI in the film does not follow any of the predicted trends by percolation theory or the LAS equation. Inaccurate film thickness estimations might have influenced the NDI concentrations altering the electron diffusion. Even though SEM is very accurate, the sampling method was very unreliable for the film thickness could vary much within the same film to estimate the film thickness more accurately atomic force microscopy (AFM) or ellipsometry are promising techniques. These techniques can cover larger surface areas for a better average thickness. Also the alteration in the concentration of the redox active linker led to structural changes in the film. The incorporation of the less soluble dcphMe–BiPy linker resulted in unstable materials and unpredictable incorporation ratios. Exploring different redox inactive linker options that are of the same length and display similar solubility characteristics as dcphOH–NDI. This approach might prove tedious and expensive for new linker synthesis have to be developed. There are however other techniques to analyse the electroactivity without having to grow a thin film. Since the bulk powder did form it could be used to analyse the electronic properties more thoroughly. Drop casting is a often used method where a MOF suspension is deposited onto an electrode and the solvent is allowed to evaporate. But delamination is often a problem.[31] Using Carbon (graphite) and MOF powder to make a paste which is smeared onto an electrode could also be a possibility.[32] Nafion might also be a viable option as it acts as an adhesive additive in a mixture of a carbon/MOF paste due to its polymeric nature. At the same time Nafion might increase electroactive performance of the analyte because of its proton conductor properties that stabilize negative charges.[33]

Catalyst loadings. For future catalyst incorporation it is important that the catalyst incorporated can act to its full potential in the MOF, meaning: the electron transfer in the MOF must be faster than the collective TOF of the catalyst. In other words, the collective TOF or demand for electrons must be lower than the electron transfer rate. Leaving substrate and stability issues aside, in case of highly active

catalysts the loading might never reach the percolation threshold before the electron transfer starts to impede the activity of the catalyst because it could not keep up with the demand for electrons. When considering a HER catalysed by Fe–Fe hydrogenase[13] for example, larger amounts of catalyst, in an excess of substrate, the bigger quantity of hydrogen is produced. This would lead to the assumption that with more catalyst in the framework more hydrogen can be produced. But, this is only true when the electron hopping mechanism is as fast or faster than the speed at which the catalyst turns over. In optimal electron hopping conditions the ratio between the catalyst and NDI can not exceed one over the TOF of the catalyst divided by the speed at which the redox–active framework transfers electrons which could be rate determined by counterion diffusion.[4]

This statement, formulated in an equation is derived from the characteristic current density[34] as such:

$$\frac{C(NDI)}{C(Cat)} \geq \frac{df^2 k_{Cat}}{D_e} \quad (3.1)$$

were D_e ($\text{cm}^2 \text{ s}^{-1}$) is the formal electron diffusion coefficient, k_{Cat} the reaction kinetics (s^{-1}) and df (cm) the film thickness. The ratio between the catalyst to NDI corresponds to the concentration ($C_{(Cat)/(NDI)}$). The diffusion coefficient corresponds to a one electron transfer or self exchange rate between NDI charge carrier and k_{Cat} corresponds to the TOF of the catalyst for an one electron process.

Film thickness. Eq. 3.1 is an oversimplified equation, because it assumes the electron transfer between the charge carrier and the catalyst to be not the rate limiting step and that the substrate concentration remains constant during catalyses via the electron relay. Furthermore, equation 3.1 only describes an one electron transfer were for hydrogen evolution two are required. It does however, present the relationship between the ratio of catalyst and the formal electron diffusion coefficient D_e to the film thickness. Ions need to travel through the framework to stabilize the reduced NDI. The diffusion of ions through a framework depends on how big the pores are, i.e., what kind of MOF film and how far they need to diffuse in, i.e., the thickness of the film. Thus, The film thickness and structural similarity between samples has a large influence on the overall catalytic activity. Optimisation of the formal electron diffusion (D_e) is in a tight relationship with the film structure and thickness as shown in by equation 3.1 and in the Cottrel equation. The thickness of MOFs is currently investigated in the Ott. group by growing MOFs layer by layer with alternating linker and metal ion solutions in solvothermal conditions.

Ongoing work. This work represents an important step for the development electrocatalysis in Redox–active MOFs. Future work will be conducted on the modification of the bipyridine moiety of the 16% BiPY incorporated bulk MOF with cobalt.[22][23] to study the catalytic activity optimistically as a result of the electron transfer between the charge carrier and a catalyst.

4. Experimental section

4.1 Materials and Synthesis

4.1.1 Materials

All chemicals for synthesis were used as received without further purification and have been listed in table (4.1)

Table 4.1: List of the chemicals

Chemicals	Purity %	Supplier
ZrCl ₄	99,99	Sigma-Aldrich
4-amino-3-hydroxy-benzoic acid	97	Fluorochem
Naphthalene-1,4,5,8-tetracarboxylic acid dianhydride	98	TCI
DMF	99,9	VWR
glacial acetic acid	99,9	VWR
5,5'-dibromo-2,2'-Bipyridine	99	Fluorochem
(4-(Methoxycarbonyl)-3-methylphenyl)boronic acid	99	Fluorochem
Tetrakis(triphenylphosphine)Palladium(0)	99	Sigma-Aldrich
DME	99	Sigma-Aldrich
Chloroform 0,6% ethanol stabilized	99,1	Merck
THF	99,9	Merck
MeOH	99,9	Merck

The fluorine doped tin oxide FTO substrate for the thinfilm MOF synthesis were purchased from Sigma-Aldrich. ¹H NMR spectra were obtained from a JEOL 400 MHz spectrometer at 293 K. The chemical shift were internally referenced to proton residue signal from the deuterated solvent on ppm. Prior to MOF analyses with NMR the sample of 10 mg with 0.575 mL of DMSO-d₆ is digested with the addition of 25 μL HF 46% in water.

4.1.2 Synthesis

DcphOH-NDI. 3-Hydroxy-2-[7-(4-carboxy-2-hydroxyphenyl)-1,3,6,8-tetraoxo-3,6,7,8-tetrahydro-1H-benzo[*lmn*][3,8]phenanthroline-2-yl]benzoic acid was synthesized following an adapted reported procedure.[4] A round bottom flask was charged with 2,2 eq, 4-amino-3-hydroxy-benzoic acid 1.01 gram (6,6 mmol), naphthalene-1,4,5,8-tetracarboxylic dianhydride 0,804 gram (3 mmol) and DMF (20 mL). The reaction mixture was refluxed over night under Ar atmosphere. Once the reaction flask was cooled to room temperature 5 mL 1 M HCl was added and the crude product was precipitated by dropping the reaction mixture in ice-cooled water (250 mL). The precipitate was collected, washed with 25 mL each ethanol, water and ether with a glassfrit filtration and dried under vacuum. Yield: 1,04g

(66%). $^1\text{H NMR}$ (400MHz, DMSO-d_6) (δ) ppm: 7.43—7.49 (m, 2 H) 7.50—7.56 (m, 2 H) 7.56—7.60 (m, 2 H) 8.59—8.88 (m 4 H) 10.17 (s, 2 H)

DcphMe–BiPy. 4,4'–(2,2'–bipyridine–5,5'–diyl)–3,3'–dimethyl–dibenzoic acid was synthesized using a Suzuki coupling using a microwave and a saponification reaction. A mixture of DME and saturated sodium bicarbonated solution 14:6 mL was degassed. The microvial was charged with Palladium(PPh_3)₄ (23 mg, 0,017), boronic acid (371 mg, 1,92 mmol) and dibrombipyridine (200 mg, 0,637 mmol) and reacted in a microwave at 150° C. After cooling to RT the crude material washed with ice water and extracted with chloroform with a Soxhlet extraction overnight. The chloroform was removed and an NMR was taken of the white product after which it was refluxed in a solvent mixture of 10 mL 6 M NaOH solution 5 mL methanol and Tetrahydrofuran overnight. The pH was neutralized and the white precipitate was dried under vacuum. Yield: 43.1mg (14.8%). $^1\text{H NMR}$ (400MHz, DMSO-d_6) (δ) ppm: 7.43—7.49 (m, 2 H) 7.50—7.56 (m, 2 H) 7.56—7.60 (m, 2 H) 8.59—8.88 (m 4 H) 10.17 (s, 2 H)

Zr(dcphOH–NDI PIZOF BULK Synthesis. The MOF was synthesized following the reported procedure by Johnson et al. (2018). In a 20 mL vial with a Teflon protected cap ZrCl_4 (82 mg 0,35 mmol), dcphOH–NDI (188,4 mg (0.35 mmol) and 0,602 mL (10,5 mmol) of glacial acetic acid were combined in 4 mL DMF. The mixture was sonicated for 10 minutes and heated for 72 h in a preheated oven on 120 C °. The dark yellow precipitate is collected and washed 3 times with DMF by centrifugation followed by incubation of 24 h in DMF. The solvent was exchanged with Methanol via the same procedure and stored for further use. The pale yellow powder was dried in air for PXRD and SEM analyses and activated under vacuum at 85 C ° for 12 h for gas adsorption analyses.

Zr(dcphMe–bipy Zr(dcphOH–NDI) mix MOF BULK Synthesis. The MOF was synthesized following and adapted procedure reported by Johnson. A 7 mL vial with a Teflon cap was charged with ZrCl_4 55 mg (0,24 mmol) dcphMe–BiPy (20 mg 0,048 mmol) dcphOH–NDI (103,7 mg, 0,192 mmol) Acetic acid (0,619 mL 45 equivalent) and 4 mL of DMF to yield and 80% redox active MOF. After 10 min of sonicating the vial was heated for 3 days at 120. Once the vial was cooled down, the precipitate was centrifuged washed 3 times and incubated for 24 hours in DMF. The solvent was exchanged for Methanol using the same washing procedure for storage until further use.

Zr(dcphOH–NDI)@FTO PIZOF Thin Film Synthesis. The Thin Film MOF was synthesized following the reported procedure by Johnson et al. (2018). The 2 by 1 cm² slides were submerged in a 1 mM of dcphOH–NDI in DMF overnight to form a self assembled monolayer (SAM). A 8 mL of DMF solution was prepared with ZrCl_4 (23,3 mg 0,10 mmol), dcphOH–NDI (53,8 mg 0,10 mmol) and 171 μL in a 20 mL vial. After 10 minutes of sonication the FTO slide was inserted to the vial and placed in a preheated oven at 120 C ° for 72 h. The vial was allowed to cool down and the MOF thin film was washed with 3 mL of ethanol and DMF each and submerged in DMF till further use.

Zr(dcphOH–NDI/dcphMe–BiPY)@FTO MOF Thin Film Synthesis. Using the reported procedure for thin film synthesis by Johnson. In 20 mL scintillation vials ZrCl_4 , dcphOH–NDI, dcphMe–BiPy and 30 eq. of glacial acetic acid were combined in 8 mL DMF and sonicated for 10 minutes to make 80, 50 and 20% OH–NDI MOF precursor solutions see table 4.2 below. Clean FTO slides of 2 by 1 cm were allowed to soak in 1 mM dcphOH–NDI overnight to form a self-assembled monolayer (SAM). A SAM–modified FTO slide was inserted in the scintillation vial and heated for 3 days at 120° C. The vials were allowed to cool to RT and the films were washed with DMF and stored in DMF for further use. The remaining powder was washed with 3 times with DMF and EtOH and allowed to dry to air till further use.

Table 4.2: summary of the Mixed linker MOF solutions of 80, 50 and 20% for thin film synthesis

	ZrCl ₄	dcphMe–BiPY	dcphOH–NDI
(A)80% NDI	23,3 mg (0,1 mmol)	9,09 mg (0,02 mmol)	43 mg (0,08 mmol)
(B)80% NDI	11,65 mg (0,05 mmol)	4,5 mg (0,01 mmol)	21,5 mg (0,04 mmol)
(C)50% NDI	23,3 mg (0,1 mmol)	22,72 mg (0,05 mmol)	26,85 mg (0,05 mmol)
(D)20% NDI	23,3 mg (0,1 mmol)	36,36 mg (0,08 mmol)	10,74 mg (0,02 mmol)

4.1.3 Methodes and Procedures

Degasing. The removal of oxygen is done by purging solvents or solutions with gas, bubbling either argon or nitrogen through. A more thorough way is use the freeze pump thaw method. This method makes use of the equilibrium of gas dissolved and in the headspace of the solvent. upon freezing the solution as the name implies with liquid nitrogen and allowing it to thaw under static vacuum, gas develops as a result of low pressures while keeping evaporation to a minimal due to the low temperature.

Fluorine doped tin oxide, thin films preparation. The Thin Film MOF was synthesized following the reported procedure by Johnson et al. (2018). FTO slides where purchased from Sigma–Aldrich and stored in the dark. The glas was cut with a glas cutter in pieces of 2 by 1 cm. The slides where thoroughly washed by sonication in a solution of alkonox, 100% ethanol and acetone successively, blown dry between each step with a N₂ flow.

Powder X–ray Diffraction. Approximately 40 mg of the sample is smeared thin and evenly on the sample holder. The holder is locked in to a Simons D5000 diffractometer (Cu K α λ = 0.15418nm) equipped with parallel beam optics (mirror + mirror) for grazing–incidence XRD measurements. The sample was measured using Diffrac Plus XRD Commander at 45kV and 40 mA with a step size of 0,02°over the angle from 3 to 30 2 θ .

Scanning Electron Microscopy. The MOF samples were placed in a sample holder using conductive carbon tape to hold them in place. before the measurements the samples where coated with a Pd–Au sputter coater for 30 seconds. A Zeis 1550 Schottky field emission scanning electron microscope was used to take the SEM images. The images where collected with an InLens detector at 5 kV acceleration voltage.

Electrochemistry. Electrochemical analyses of the thin film samples were performed in a one-compartment, three electrode set up (see Figure 4.1). The thin film samples were prepared by removing the top 1/4 of the thin film MOF with a minimal amount of 2 M HCl, doped with a small amount of HCl, by rubbing the MOF off the FTO glass. The films were washed with DMF and ethanol and dried over a nitrogen flow to remove the HCl. A 50 mL electrolyte solution of 0.5 M LiClO_4 in anhydrous DMF was prepared. The cell was filled with 7 mL of electrolyte solution and degassed with argon. $\text{Ag}/\text{Ag}(\text{NO}_3)$ and a glassy carbon rod were used as reference and counter electrodes, respectively. The film was mounted on the electrode with the newly exposed FTO surface. To prevent any movement in the screw holding the film, the electrode was wrapped with Teflon tape. The working and reference electrodes were prepared using the same electrolyte solutions to complete the circuit. The analyses were initiated after one hour degassing time using an Autolab PGSTAT100 potentiostat controlled by a GPES 4.9 software (EcoChemie). During the analyses, the vessel was kept under argon flow.

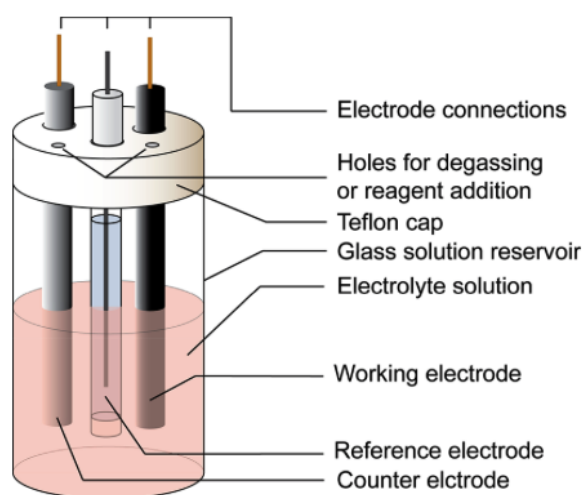


Figure 4.1: A schematic presentation of a one compartment three electrode setup.[5]

5. *Acknowledgements*

First of all, I would like to express my sincere gratitude to **Prof. Sascha Ott** for the opportunity to do my bachelor graduation project at the University of Uppsala.

Secondly, I would like to pay my gratitude to the PhD students: **Ashleigh Castner** and **Ben Johnson** for their time and effort to show me new techniques and guide me in the learning process.

Special thanks to the MOF group from whom I have learned so much and whose members always made some time for me and my questions.

Special thanks to **Brian McCarthy** who helped me work safely with hydrofluoric acid.

and Special thanks to the Master students with whom I could share idea's and drinks.

Rebekka Meyer: I would like to thank for her help in learning to work with Latex.

Thomas Pierru: Thanks for helping me with rearranging equations.

Lastly a sincere thank you to all colleagues responsible for the light mood, healthy work environment and happy hallway chatter.

Bibliography

- [1] Jasmina Hafizovic Cavka, Søren Jakobsen, Unni Olsbye, Nathalie Guillou, Carlo Lamberti, Silvia Bordiga, and Karl Petter Lillerud. A new zirconium inorganic building brick forming metal organic frameworks with exceptional stability. *Journal of the American Chemical Society*, 130(42):13850–13851, 2008.
- [2] Shuai Yuan, Liang Feng, Kecheng Wang, Jiandong Pang, Matheiu Bosch, Christina Lollar, Yujia Sun, Junsheng Qin, Xinyu Yang, Peng Zhang, et al. Stable metal–organic frameworks: design, synthesis, and applications. *Advanced Materials*, 30(37):1704303, 2018.
- [3] Lynne S Taylor and George Zografi. The quantitative analysis of crystallinity using ft-raman spectroscopy. *Pharmaceutical research*, 15(5):755–761, 1998.
- [4] Ben A Johnson, Asamanjoy Bhunia, Honghan Fei, Seth M Cohen, and Sascha Ott. Development of a uio-type thin film electrocatalysis platform with redox-active linkers. *Journal of the American Chemical Society*, 140(8):2985–2994, 2018.
- [5] Noémie Elgrishi, Kelley J Rountree, Brian D McCarthy, Eric S Rountree, Thomas T Eisenhart, and Jillian L Dempsey. A practical beginner’s guide to cyclic voltammetry. *Journal of chemical education*, 95(2):197–206, 2017.
- [6] Janette M Hudson, Kerensa Heffron, Violetta Kotlyar, Yelizaveta Sher, Elena Maklashina, Gary Cecchini, and Fraser A Armstrong. Electron transfer and catalytic control by the iron- sulfur clusters in a respiratory enzyme, e. coli fumarate reductase. *Journal of the American Chemical Society*, 127(19):6977–6989, 2005.
- [7] Masahiko Hirano, Kazuhiko Satoh, and Sakae Katoh. The effect on photosynthetic electron transport of temperature-dependent changes in the fluidity of the thylakoid membrane in a thermophilic blue-green alga. *Biochimica et Biophysica Acta (BBA)-Bioenergetics*, 635(3):476–487, 1981.
- [8] Scott A Trammell and Thomas J Meyer. Diffusional mediation of surface electron transfer on tio2. *The Journal of Physical Chemistry B*, 103(1):104–107, 1999.
- [9] David N Blauch and Jean Michel Saveant. Dynamics of electron hopping in assemblies of redox centers. percolation and diffusion. *Journal of the American Chemical Society*, 114(9):3323–3332, 1992.
- [10] Hailian Li, Mohamed Eddaoudi, Michael O’Keeffe, and Omar M Yaghi. Design and synthesis of an exceptionally stable and highly porous metal-organic framework. *nature*, 402(6759):276, 1999.
- [11] Liang Feng, Shuai Yuan, Jun-Sheng Qin, Ying Wang, Angelo Kirchon, Di Qiu, Lin Cheng, Sherzod T Madrahimov, and Hong-Cai Zhou. Lattice expansion and contraction in metal-organic frameworks by sequential linker reinstallation. *Matter*, 2019.

- [12] Hiroyasu Furukawa, Kyle E Cordova, Michael O’Keeffe, and Omar M Yaghi. The chemistry and applications of metal-organic frameworks. *Science*, 341(6149):1230444, 2013.
- [13] Sonja Pullen, Honghan Fei, Andreas Orthaber, Seth M Cohen, and Sascha Ott. Enhanced photochemical hydrogen production by a molecular diiron catalyst incorporated into a metal–organic framework. *Journal of the American Chemical Society*, 135(45):16997–17003, 2013.
- [14] Kuen-Song Lin, Abhijit Krishna Adhikari, Chi-Nan Ku, Chao-Lung Chiang, and Hua Kuo. Synthesis and characterization of porous hkust-1 metal organic frameworks for hydrogen storage. *international journal of hydrogen energy*, 37(18):13865–13871, 2012.
- [15] Markus Tonigold, Ying Lu, Björn Bredenkötter, Bernhard Rieger, Stefan Bahnmüller, Julia Hitzbleck, Gerhard Langstein, and Dirk Volkmer. Heterogeneous catalytic oxidation by mfu-1: A cobalt (ii)-containing metal–organic framework. *Angewandte Chemie International Edition*, 48(41):7546–7550, 2009.
- [16] Kuppuswamy Kalyanasundaram, John Kiwi, and Michael Grätzel. Hydrogen evolution from water by visible light, a homogeneous three component test system for redox catalysis. *Helvetica Chimica Acta*, 61(7):2720–2730, 1978.
- [17] Mohammad Al Kobaisi, Sidhanath V Bhosale, Kay Latham, Aaron M Raynor, and Sheshanath V Bhosale. Functional naphthalene diimides: synthesis, properties, and applications. *Chemical reviews*, 116(19):11685–11796, 2016.
- [18] E Laviron, L Roullier, and C Degrand. A multilayer model for the study of space distributed redox modified electrodes: Part ii. theory and application of linear potential sweep voltammetry for a simple reaction. *Journal of Electroanalytical Chemistry and Interfacial Electrochemistry*, 112(1):11–23, 1980.
- [19] Fred C Anson, David N Blauch, Jean Michel Saveant, and Ching Fong Shu. Ion association and electric field effects on electron hopping in redox polymers. application to the tris (2, 2’-bipyridine) osmium (3+)/tris (2, 2’-bipyridine) osmium (2+) couple in nafion. *Journal of the American Chemical Society*, 113(6):1922–1932, 1991.
- [20] Pierre Bonhôte, Eric Gogniat, Sophie Tingry, Christophe Barbe, Nicolas Vlachopoulos, Frank Lenzmann, Pascal Comte, and Michael Grätzel. Efficient lateral electron transport inside a monolayer of aromatic amines anchored on nanocrystalline metal oxide films. *The Journal of Physical Chemistry B*, 102(9):1498–1507, 1998.
- [21] David N Blauch and Jean Michel Saveant. Effects of long-range electron transfer on charge transport in static assemblies of redox centers. *The Journal of Physical Chemistry*, 97(24):6444–6448, 1993.
- [22] David P Hickey, Christopher Sandford, Zayn Rhodes, Tobias Gensch, Lydia R Fries, Matthew S Sigman, and Shelley D Minter. Investigating the role of ligand electronics on stabilizing electrocatalytically relevant low-valent co (i) intermediates. *Journal of the American Chemical Society*, 141(3):1382–1392, 2019.
- [23] Ziqiang Lei, Xiangen Han, Yulai Hu, Rongmin Wang, and Yunpu Wang. Synthesis and catalytic oxidation properties of polymer-bound cobalt complexes. *Journal of applied polymer science*, 75(8):1068–1074, 2000.

- [24] Bjørnar Arstad, Helmer Fjellvåg, Kjell Ove Kongshaug, Ole Swang, and Richard Blom. Amine functionalised metal organic frameworks (mofs) as adsorbents for carbon dioxide. *Adsorption*, 14(6):755–762, 2008.
- [25] Dawei Feng, Zhi-Yuan Gu, Jian-Rong Li, Hai-Long Jiang, Zhangwen Wei, and Hong-Cai Zhou. Zirconium-metalloporphyrin pcn-222: mesoporous metal–organic frameworks with ultrahigh stability as biomimetic catalysts. *Angewandte Chemie International Edition*, 51(41):10307–10310, 2012.
- [26] Ross J Marshall, Yaroslav Kalinovsky, Sarah L Griffin, Claire Wilson, Barry A Blight, and Ross S Forgan. Functional versatility of a series of zr metal–organic frameworks probed by solid-state photoluminescence spectroscopy. *Journal of the American Chemical Society*, 139(17):6253–6260, 2017.
- [27] Andreas Schaate, Pascal Roy, Adelheid Godt, Jann Lippke, Florian Waltz, Michael Wiebcke, and Peter Behrens. Modulated synthesis of zr-based metal–organic frameworks: from nano to single crystals. *Chemistry–A European Journal*, 17(24):6643–6651, 2011.
- [28] Shaoyang Lin, Yuliana Pineda-Galvan, William A Maza, Charity C Epley, Jie Zhu, Matthew C Kessinger, Yulia Pushkar, and Amanda J Morris. Electrochemical water oxidation by a catalyst-modified metal–organic framework thin film. *ChemSusChem*, 10(3):514–522, 2017.
- [29] Omar K Farha and Joseph T Hupp. Rational design, synthesis, purification, and activation of metal-organic framework materials. *Accounts of chemical research*, 43(8):1166–1175, 2010.
- [30] Jeanne L Bolliger and Christian M Frech. Dichloro-bis (aminophosphine) complexes of palladium: Highly convenient, reliable and extremely active suzuki–miyaura catalysts with excellent functional group tolerance. *Chemistry–A European Journal*, 16(13):4075–4081, 2010.
- [31] Amir H Khoshaman and Behraad Bahreyni. Application of metal organic framework crystals for sensing of volatile organic gases. *Sensors and Actuators B: Chemical*, 162(1):114–119, 2012.
- [32] Yang Wang, Yichun Wu, Jing Xie, and Xiaoya Hu. Metal–organic framework modified carbon paste electrode for lead sensor. *Sensors and Actuators B: Chemical*, 177:1161–1166, 2013.
- [33] Yang Wang, Huali Ge, Guiqin Ye, Huanhuan Chen, and Xiaoya Hu. Carbon functionalized metal organic framework/nafion composites as novel electrode materials for ultrasensitive determination of dopamine. *Journal of Materials Chemistry B*, 3(18):3747–3753, 2015.
- [34] Cyrille Costentin and Jean-Michel Savéant. Cyclic voltammetry of electrocatalytic films: fast catalysis regimes. *ChemElectroChem*, 2(11):1774–1784, 2015.

6. Appendices

6.1 Appendix 1

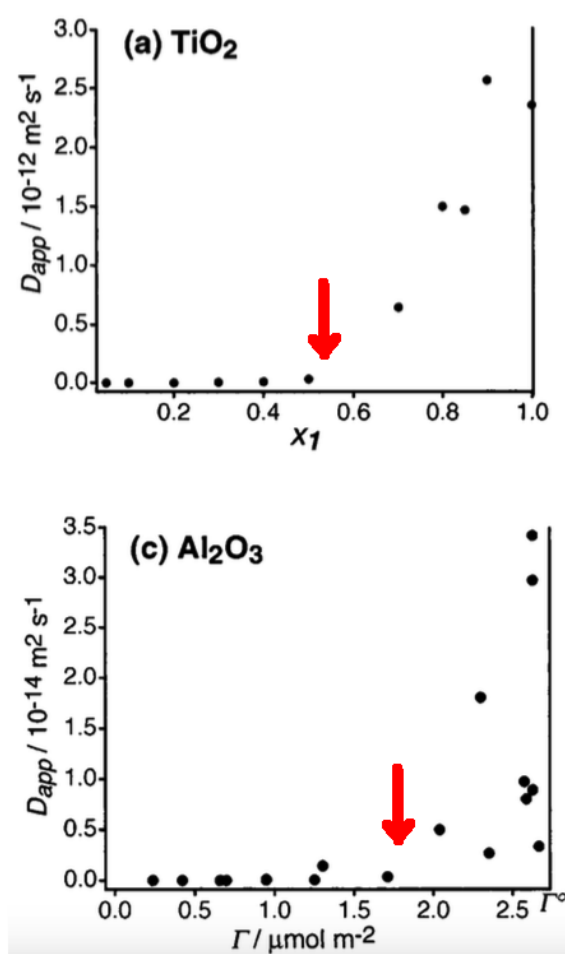


Figure 6.1: Formal electron diffusion (D_{app}) as a function of surface coverage of a redox active monolayer on conductive films (a) TiO_2 , (c) Al_2O_3 in $\mu\text{mol/m}^2$ following a potential step from 0,2 to 1,0 v. The red arrow points a the onset of electron transfer.

6.2 Appendix 2

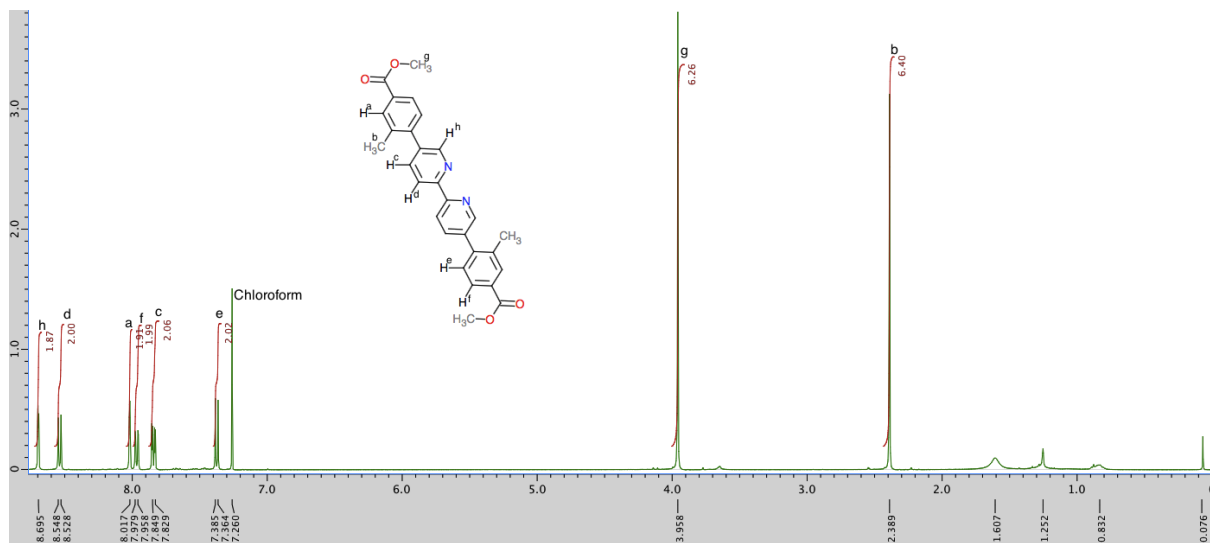
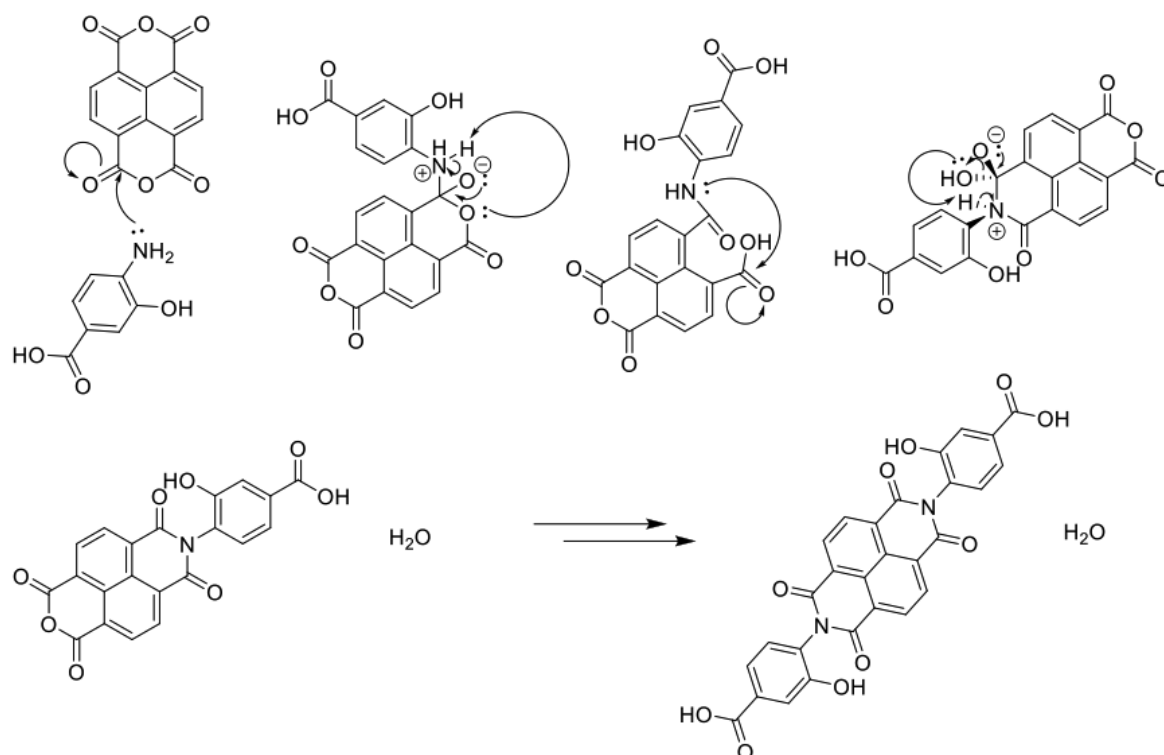


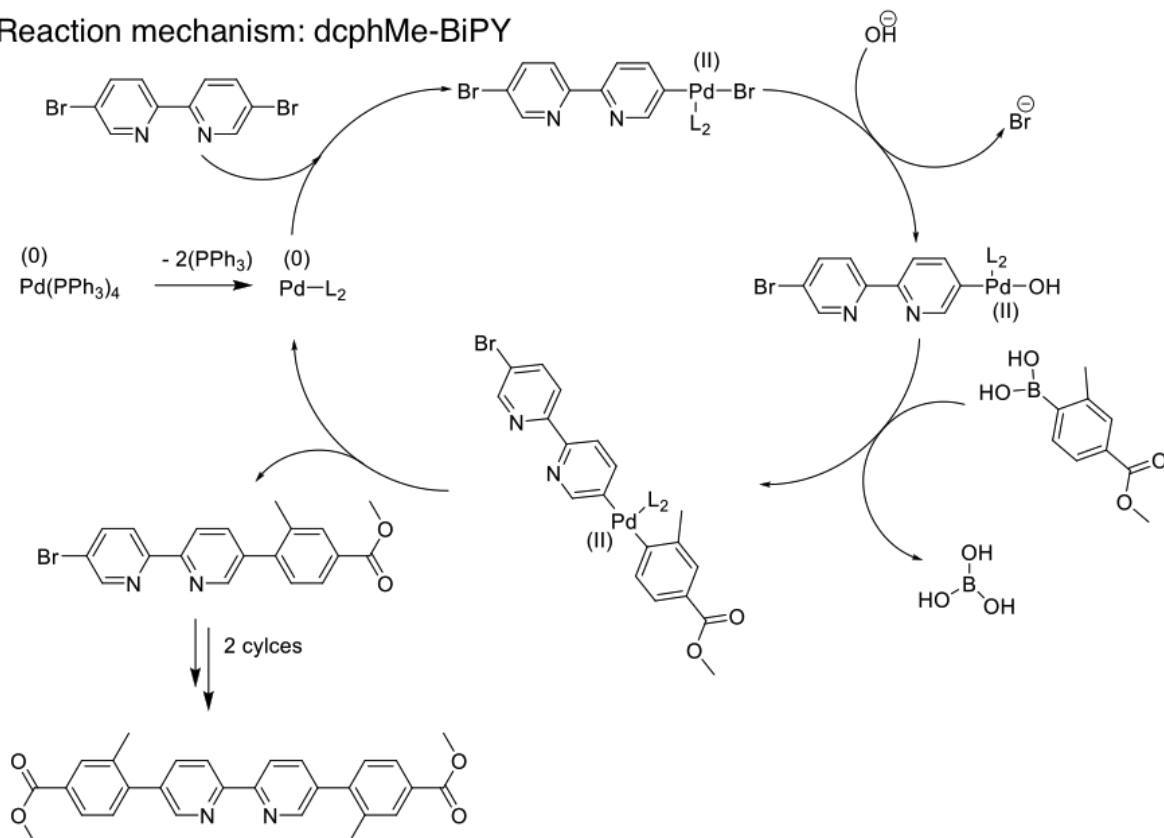
Figure 6.2: NMR of the ester protected dcpHMe-BiPy

6.3 Appendix 3

Reaction mechanism: dcpH-NDI



Reaction mechanism: dcpMe-BiPY



6.4 Appendix 4

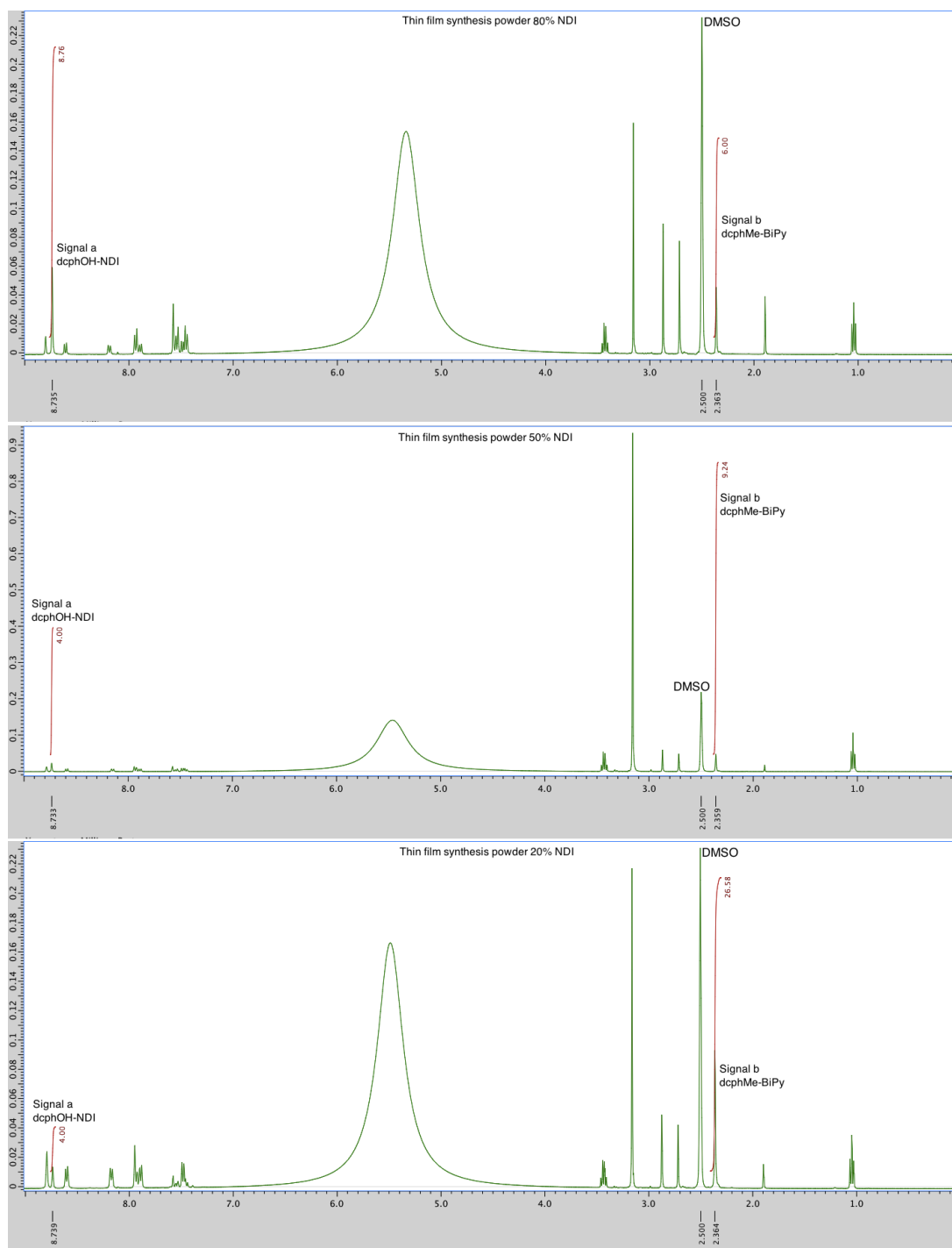


Figure 6.3: NMR of digested MOF powders resulting from the mixed thin film synthesis

From the ratio between the signals integrated the ratio of NDI incorporated is calculated: 54%, 65% and 23% NDI in the B, C and D thin film powder respectively.

6.5 Appendix 5

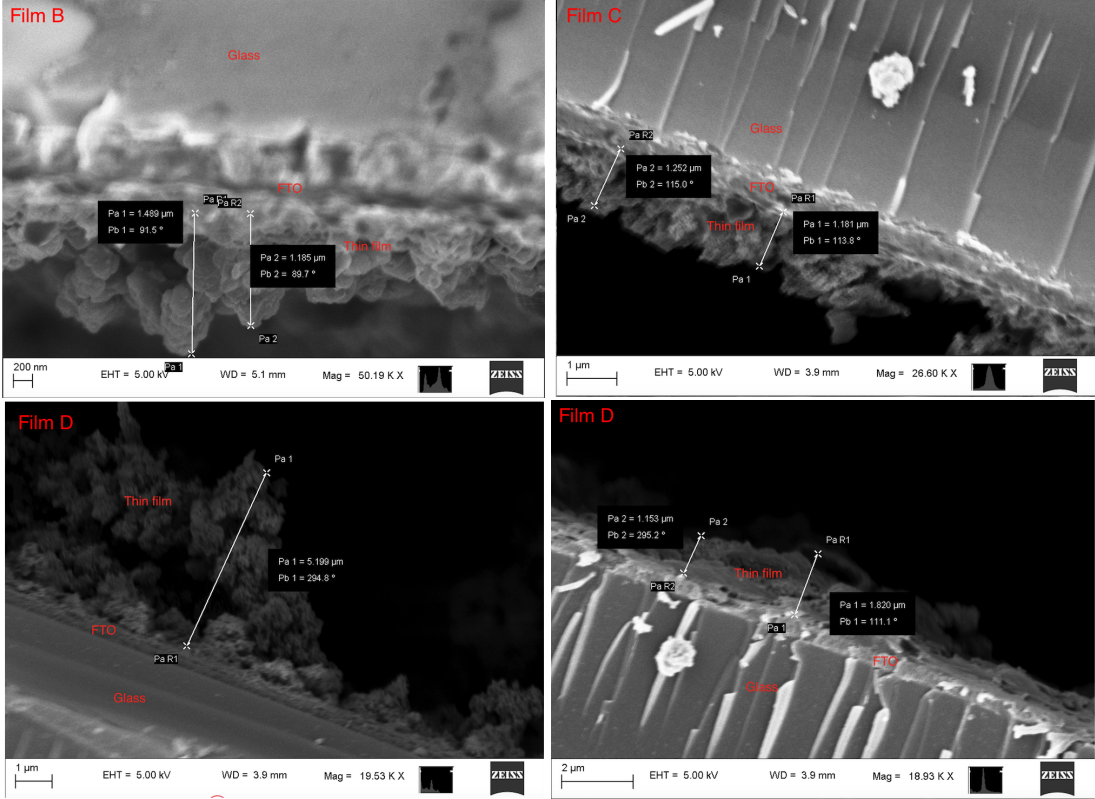


Figure 6.4: SEM images of the crossection of the thin films B, C, D

The film thickness of the films was determined by taking an average of the thickness measured in the software. 100% NDI film = 1 [4], film B = 1,337 , film C = 1,2165 and film D = 3,343 μm

6.6 Appendix 6

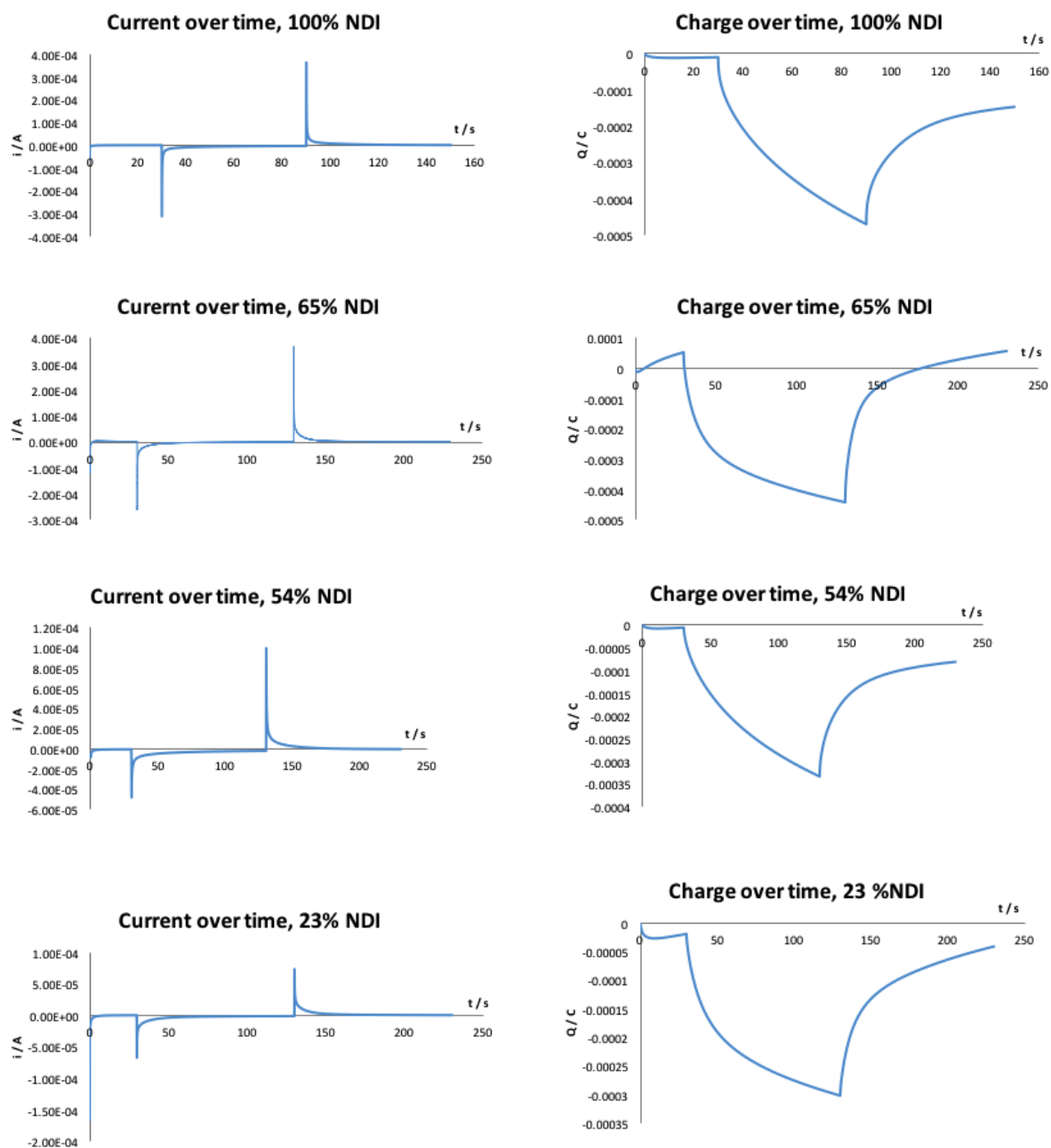


Figure 6.5: Coulometry data of film B, C D, and the 100% film